Diploma thesis

Evaluating the degradation behaviour of magnesium-lithium-based alloy in rats

submitted by

Sandra Gieringer

for the Academic Degree of

Doctor medicinae universae

(Dr. med. univ.)

at the

Medical University of Graz

conducted at the

Department of Orthopaedics and Trauma

under the supervision of

Univ.-Ass. Nicole Sommer, PhD

and

Assoz.-Prof. Priv.-Doz. Dr.med.univ. Annelie-Martina Weinberg

Graz, 10.06.2022

Statutory Declaration

I hereby declare that I have authored this diploma thesis fully on my own, that I have not used any other than the declared sources, and that I have explicitly marked all material which has been quoted either literally or by content from the used sources.

Graz, 10.06.2022 *Sandra Gieringer, eh.*

Danksagungen

Zuallererst möchte ich mich bei meiner Betreuerin **Univ.-Ass. Nicole Sommer, PhD** für die ausgezeichnete Begleitung während der Erstellung dieser Arbeit bedanken. Vor allem ihre Expertise und der offene Raum für Fragen, besonders in der Anfangszeit, waren eine Bereicherung für meinen Werdegang. Nicht unerwähnt soll meine betreuende Professorin **Assoz.-Prof. Priv.-Doz. Dr.med.univ. Annelie-Martina Weinberg** bleiben, bei welcher ich mich auch für ihre Unterstützung herzlich bedanken möchte.

Es ist mir außerdem eine Herzensangelegenheit meiner Familie zu danken, welche mich durch diese außergewöhnliche Zeit begleitet und mir dieses Studium erst ermöglicht hat.

Herzlichen Dank!

Contents

List of abbreviations

SD	Standard Deviation
Ca	Calcium
Mg	Magnesium
HE	hematoxylin eosin
PTH	Parathyrin
i.e.	id est, das heißt
M-CSF	macrophage colony stimulating factor
CSF	colony stimulating factor
OPG	Osteoprotegerin
RANK	receptor activator of NF-kB
RANKL	receptor activator of NF-kB ligand
IL 1, 6, 8	Interleukin 1, 6, 8
IGF 1, 2	Insulin-like growth factor 1, 2
TGF-ß	Transforming growth factor beta
PIO	peri-implant osteolysis
LiCPP	lithium doped calcium phosphate scaffold
Nf-kB	nuclear factor kappa light chain enhancer of activated B cells
VEGF	vascular endothelial growth factor
PDGF	platelet derived growth factor
PEGF	precursor epidermal growth factor
BMDS	bone marrow derived stem cells
Li	lithium
Ti	titan
TNF-α	tumor necrosis factor-α
BMP	bone morphogenic protein
VEGF	vascular endothelial growth factor
HIF-1α	hypoxia-inducible factor 1-alpha
MMP	matrix-metalloproteases
DXA	dual-energy x-ray absorptiometry
SMAD	small mother against decapentaplegic
3D	three-dimensional
HU	Hounsfield Units
LX41	Mg-4Li-1Ca alloy

List of figures

List of tables

Zusammenfassung

Osteoporose ist eine Erkrankung, die bevorzugt die Altersklasse über 65 betrifft. Der osteoporotische Knochen nimmt sowohl in seiner Dichte, als auch in seiner Härte ab. Die chirurgische Versorgung osteoporotischer Frakturen wird mit Standardmaterialien wie Titan oder Stahl durchgeführt, welche aufgrund ihrer guten Verträglichkeit, Rigidität und Biokompatibilität weit verbreitet sind. Nichtsdestotrotz können diese permanente Materialien „stress-shielding“ verursachen, wodurch Re-frakturen unterhalb des Implantates begünstigt werden. An dieser Stelle tritt Magnesium (Mg) als innovatives Material in den Vordergrund. Mg weist gute biomechanische und resorbierbare Eigenschaften mit guter Verträglichkeit auf. Studien haben bereits gezeigt, dass die Freisetzung von Mg-Ionen während der Korrosion die Knochenbildung und die Expression von anabolen Markern im peri-implantären Knochen unterstützt. Vorstudien im osteoporotischen Rattenmodell haben gezeigt, dass das Mg-basierte Material ZX00 (Mg-Zink-Kalzium) jedoch schneller degradiert als im jungen Tier. Ziel dieser Studie war es, die neue, stabilere Magnesium-Kalzium-Lithium basierte Legierung LX41 mit ZX00 zu vergleichen, welche vorab in gesunde, wachsende Ratten implantiert wurde.

Für die Studie wurden zylindrische LX41 Pins transkortikal in die proximale Metaphyse der Tibia juveniler Ratten implantiert. Direkt nach der Implantation, sowie nach 2, 12, 18 und 24 Wochen wurden Mikro-(μ)CT Bilder der eingesetzten Pins angefertigt. Nach der 3D-Rekonstruktion wurde das Implantatvolumen, die Implantatoberfläche und die Wasserstoffbildung evaluiert. Zur Beurteilung der Knochenmorphologie wurden die Knochen nach der Euthanasie fixiert, eingebettet und histologisch beurteilt.

Die Ergebnisse zeigen einen initial höheren Volumenverlust von LX41 bis zur 18. Woche, welcher dann langsam ein Plateau erreicht. Zwei Wochen nach Implantation wurde eine vermehrte Gasentwicklung beobachtet, welche in den weiteren Messpunkten auf ein niedriges, adäquates Niveau absank. Der Knochenmarkraum blieb intakt und eine gute Osteointegration und Knochenneubildung wurde histologisch festgestellt. Weiters zeigten sich keine Anzeichen für eine akute Entzündung oder Granulombildung im Knochen.

Die Ergebnisse dieser Studie zeigen, dass die neu entwickelte LX41 Legierung trotz anfänglicher Zunahme der Wasserstoffgasbildung und -menge weder einen negativen Einfluss auf die Frakturheilung noch auf die Knochenneubildung hatte. LX41 zeigt dadurch sein mögliches Potenzial als bioresorbierbares Material für die Anwendung in der Orthopädie. Weitere Studien werden benötigt, um die Anwendbarkeit von LX41 im osteoporotischen Knochen zu zeigen.

Abstract

Osteoporosis is a disease that primarily affects people over 65. Osteoporotic bone decreases in both density and stiffness. Surgical treatment of osteoporotic fractures is performed with standard materials like titanium or steel, which are commonly used due to their good tolerance, rigidity and biocompatibility. Nevertheless, these permanent materials can induce stress-shielding, which favours re-fractures underneath the implant, trigger infections, and are usually removed after healing in a secondary operation. Magnesium (Mg) is an innovative material with good biomechanical and resorbable properties and is well tolerated. Studies have already shown that the release of Mg ions during corrosion supports bone formation and the expression of anabolic markers in peri-implant bone.

Preliminary studies on rat bones have shown that the Mg-based material ZX00, which consists of magnesium-zinc-calcium, degrades faster in osteoporotic compared to juvenile rats.

The aim of this study was to compare the new magnesium-calcium-lithium-based alloy LX41 with ZX00 in a juvenile, healthy rat model.

Seven four-weeks-old Sprague Dawley rats underwent bilateral transcortical implantation of cylindrical LX41 pins into the proximal metaphysis of the tibia. Micro (μ)-CT were performed immediately after surgery as well as 2, 12, 18 and 24 weeks afterwards. We evaluated implant volume and surface area as well as hydrogen gas formation. After sacrification, tibiae were excised, embedded and histologically analysed. The results showed an initial increased volume loss of LX41 until week 18, which decreased until week 24. Two weeks after implantation, an increased gas development was found, which decreased to low, adequate gas values at further points. Despite gas development, the bone marrow cavity appeared intact. Good osseointegration and new bone formation were histologically observed. Furthermore, there were no signs of acute inflammation or granuloma formation in the bone tissue.

In conclusion, we demonstrated that LX41 had no negative effect on bone formation, despite initially high hydrogen gas formation and quantity. The first attempt demonstrated the LX41's suitability as a bioresorbable material for orthopaedics and trauma surgery. Further studies are needed to evaluate the applicability under osteoporotic conditions.

1 Introduction

The history of biodegradable implants, especially magnesium (Mg)-based implants, already started long ago. In 1808, Sir Humphry Davy invented the production of metallic Mg. His ground-breaking approach formed the basis for the development of biodegradable Mg-based metal implants (1). In the 19th century, the physician Edward Huse described Mg wires as ligature for bleeding vessels (1,2). During the past two centuries various surgical specialities, such as orthopaedic surgery, explored the behaviour of Mg implants, *in vitro* and *in vivo,* to create the optimal material composition. However, material research on this topic continues (1).

The interesting aspects of Mg as an implant material are its unique properties. Mg shows excellent biodegradability, biocompatibility and suitable mechanical strength, comparable to cortical bone (3). The elastic modulus of Mg (41-45 GPa) is very similar to that of cortical bone (40-57 GPa), and the density is also comparable (1.74g/cm^3 Mg, 1.9g/cm^3 bone) (4). Another positive property is the physiological metabolism, which does not produce any toxic degradation products and at the same time provides the bone itself with a nutrient medium for bone remodelling (5). The current standard materials, titanium or stainless steel, are used due to their rigidity, biocompatibility and good compatibility. Nevertheless, these materials can cause so-called stress shielding. Stress shielding is characterized by tension loss owing to an implant leading to the reduction in bone density. In elderly (>65 years), stress shielding constitutes a major issue because of a lower density and strength of their bones, which makes an adequate treatment with titanium and stainless steel difficult. Furthermore, the use of these materials can lead to postoperative infection (5). Once the bone is degraded by the load transfer to the implant, fractures can occur again underneath the implant (6). Therefore, Mg provides a good alternative to circumvent the drawbacks associated with permanent implants.

The release of Mg ions during the corrosion process supports bone formation and the expression of anabolic markers in the peri-implant bone (7). Furthermore, studies have shown that these Mg ions are subsequently stored in the cortical bone and may therefore be beneficial for patients with osteoporosis by strengthening the weak bone structure (4,8,9).

Even though the idea of an independently decomposing material appears very elegant in its execution, there were similar difficulties at the beginning. Up to now, the main problem

associated with the rapid degradation and development of gas bubbles surrounding the implant has not been satisfactorily solved yet (10).

1.1 General bone grafting

Bone is a dynamic tissue that histologically consists of three major cell types: osteoclasts, osteoblasts and osteocytes. Osteoclasts and osteoblasts behave in exactly opposite ways and thereby ensure the right balance between bone resorption and formation. Osteocytes are mature bone cells and represent the main part of bone cells. They develop from osteoblasts and are subsequently no longer capable of cell proliferation. Enclosed in the bone matrix, osteocytes maintain the bone matrix and calcium homeostasis (11–14).

1.1.1 Osteoclasts

Osteoclasts are derived from mononuclear precursor cells of the monocyte-macrophage lineage, being the only cells known to be capable of resorbing bone tissue. Osteoclastogenesis requires two cytokines, receptor activator of NF-κB ligand (RANKL) and macrophage colony stimulating factor (M-CSF), for osteoclast formation. Their soluble form is primarily produced by osteoblasts and marrow stromal cells (11). Beside the differentiation of osteoclast progenitors, M-CSF is required for osteoclast survival and cytoskeletal rearrangement (11). Osteoclasts secret hydrogen ions and cathepsin K enzyme for bone resorption. Cathepsin K digests the proteinaceous matrix and the hydrogen ions dissolve the mineral components of bone matrix by acidifying the resorption compartment beneath osteoclasts (12).

The osteoclast membrane displays integrin receptors, which bind osteoclasts to bone matrix. αvβ3 integrin is the main integrin receptor enabling bone resorption binding to bone sialoprotein and osteopontin (13). Bound osteoclasts develop a ruffled border on their bone resorbing surface via metalloproteinases and cathepsin K acidified vesicles, being transported through microtubules to fuse with the membrane. The ruffled border is capable to secret hydrogen ions (H^+) via H^+ -ATPase and induce exocytosis of cathepsin K and other enzymes in the acidifies vesicles (14).

1.1.2 Osteoblasts

Subsequently, newly formed osteoblasts are delivered from mesenchymal stem cells throughout life. As bone forming unit, osteoblasts are responsible for collagen synthesis, new bone lamellae as well as for preparing mineralization through synthesis of alkaline phosphatase (AP) and matrix vesicle formation (14).
Osteoblasts are located inside and outside the bone, under the fibrous periosteal layer. In the resting state, osteoblasts are flat and therefore they are denoted as lining cells. In their active state, osteoblasts show a cubic shape with a lot of rough endoplasmic reticulum and a large Golgi-apparatus (14). A layer of unmineralized osteoid separates the active osteoblasts from the mineralized matrix. Osteoblasts generally synthesize the osteoid, which represents the organic-chemical basic structure of new bone lamellae. After completing formation of new bone lamellae, there are three paths which an osteoblast can take. Firstly turning into an osteocyte, secondly reintegration in its active from into endosteum/periosteum and lastly to undergo apoptosis like most do (14).

1.1.3 Osteocytes

Osteocytes are former osteoblasts, fully surrounded by mineralized bone matrix. The osteocyte´s cell body is located in the lacunae and their dendritic spines in the canaliculi. However, a narrow zone (~100 nanometres) remains around each osteoclast and each dendritic spine. This zone only contains interstitial fluid and small amounts of organic matrix, which is not mineralized. The bone cavity system (lacuno-canalicular system) itself represents a network of traffic routes allowing the exchange of metabolites and nutrients between osteocytes. Osteocytes communicate with each other via gap junctions and act as mechanical sensors. When mechanical stress is applied to the bone, the fluid between the lamellae starts moving and triggers a physical stimulus. Osteocytes perceive this fluid shear stress and as a biological response, synthesize active substances that intervene in bone and mineral balance (14). One active substance that is synthesized is sclerostin. Sclerostin is a glycoprotein that is secreted in a paracrine manner and inhibits bone formation. Less mechanical stress onto the bone means more abundant sclerostin secretion. Therefore, the absence of mechanical stress, like during a long hospital stay, leads to serious loss of bone mass, especially in older people (15).

1.2 Bone growth, modeling and remodeling

Bone is a vital tissue that constantly changes. It undergoes bone growth, modeling and remodeling. Bone growth occurs longitudinally and radially throughout childhood and adolescence. Longitudinal growth occurs on the growth plates. In the epiphyseal and metaphyseal areas cartilage multiplies and is further mineralized, forming primary new bone (16).

Modeling is characterized by gradual adaptation of the skeleton. Adaption is the response to mechanical forces or physiological influences acting on the bone tissue. Wolff´s law describes the physiological modeling process. The German surgeon Julius Wolff figured out that bone adapts to the loads under which it is placed. As the load applied on a bone increases, the bone becomes stronger to withstand the applied force. The opposite can occur in exactly the same way. As the stress on a bone decreases, the bone becomes weaker and less dense (17). The modeling process may also be increased in hypoparathyroidism, renal osteodystrophy, or treatment with anabolic steroids (18).

Bone remodeling begins before birth and continues until death. Bone is continuously renewed to maintain strength and mineral homeostasis (19). Discrete packets of old bone are replaced with newly synthesized proteinaceous matrix and subsequent mineralized to form new bone.

The remodeling cycle is subdivided in four sequential phases: activation, resorption, reversal and formation (19). First osteoclasts are required for activation, this involves the activation and recruitment of mononuclear monocyte-macrophage osteoclasts precursors from the circulation. Osteocytes are mainly responsible for controlling this process. They secrete the cytokine M-CSF, which initiates the proliferation of undifferentiated precursor cells (12). The mononuclear precursor cells formed, fuse to osteoclasts. This requires a cell-cell interaction between osteoclast and osteocyte or osteoblast, in which a receptor called the receptor activator of NF-kB (RANK), located on the osteoclast precursors, comes into contact with the matching ligand RANKL on the osteocyte plasma membrane. The RANK / RANKL interaction is mandatory for the breakdown of bone matrix by osteoclasts (14). It is noteworthy that the osteocytes can also secrete the opponent, namely the soluble protein osteoprotegerin (OPG). The ratio between RANKL to OPG, IL-1, IL-6, CSF, PTH, 1, 25- dihydroxycholecalciferol and calcitonin, regulates osteoclast formation, activation and resorption (20).

During the resorption phase, calcium (Ca) compounds inside the bone must be broken down by an acid. The active osteoclast has a dense ruffled border on its resorptive front, which pumps hydrogen ions into the lacunae via H^+-ATPase proton pumps. This process is used to lower the pH value as low as 4.5. Another chemical mechanism is connected to chloride channels in the osteoclast cell membrane to mobilize bone mineral. The osteoclasts also secrete lysosomal enzymes, e.g. cathepsin K to break down the organic matrix (21) resulting in resorption pits, known as Howship´s lacunae. Finally, osteocytes phagocytize the extracted matrix fragments and after performing transcytosis, release the fragments again at the cell back side (14). The end of the resorption phase is determined by multinuclear osteoclasts undergoing apoptosis (20). Subsequently, the reversal and bone formation phase begin. Once the Howship lacunae are formed, they contain a variety of mononuclear cells, including osteocytes, monocytes, and pre-osteoblasts recruited for the onset of new bone formation (19). The coupling signals that connect the end of bone resorption with the start of bone formation are still unknown. Potential coupling signals include IGF-1, IGF-2, TGF-β, bone morphogenetic proteins, platelet-derived growth factor, or fibroblast growth factor. All coupling signal candidates display at least one of these bone matrix-derived factors. For instance, TGF-β, released from the bone matrix, directly correlates with serum osteocalcin and bone-specific alkaline phosphatase (AP). Accordingly, osteoclast resorption decreases due to the inhibition of RANKL produced by osteoblasts (22).

Finally, bone formation occurs, which actually takes approximately 4 to 6 months to complete. Osteoblasts regulate the synthesisation of new collagenous organic matrix and the mineralization of matrix by releasing small, membrane-bound matrix vesicles. These vesicles concentrate phosphate and Calcium (Ca) and enzymatically destroy mineralization inhibitors such as proteoglycans or pyrophosphate (23). Osteoblasts turn into osteocytes being surrounded by or within bone matrix. The osteocytes are endued with an extensive canalicular network connecting them to osteoblasts, bone surface lining cells and other osteocytes. Approximately, 50 to 70% of osteoblasts undergo apoptosis after completing bone formation and becoming osteocytes or bone-lining cells. Influx and efflux of mineral ions into and out of the bone extracellular fluid is regulated by bone-lining cells. Osteocytes have the ability to redifferentiate into osteoblast as a result of mechanical forces or exposure to parathyroidhormone (PTH). Resorption of old bone and formation of new bone is a balanced process in a healthy individual called bone balance. With age,

cortical and trabecular bone become thinner and porous, which is due to a slightly positive periosteal and a slightly negative trabecular bone balance (7,19).

The main function of bone remodeling is replacing older, microdamaged bone with new, healthy bone to preserve mechanical strength. Adult cortical bone has a low turnover rate of just 2 to 3% per year. Nevertheless it is high enough to maintain adequate biomechanical strength. Trabecular bone shows a higher turnover rate, more than required for maintenance of mechanical strength, but necessary for mineral metabolism.

Low levels of Ca or phosphorus can be set off by activation of osteoclast resorption or non-osteoclastic Ca influx and efflux. Some parts of newly formed bone present relatively low mineral content and are able to exchange ions more easily with the extracellular fluid to ensure Ca and phosphorus balance (19).

1.3 Calcium-phosphate homeostasis

Ca and phosphate are indispensable for skeletal mineralization and human physiology. An understanding of Ca-phosphate homeostasis is required for the physician to evaluate abnormalities of Ca and phosphate as well as metabolic skeletal disorders. Disorders of Ca-phosphate homeostasis can result in Paget´s disease with high bone density or in osteoporosis or osteomalacia with low bone density. The normal regulation of bone metabolism provides a basis for management of patients with osteoporosis that involve this homeostatic system (24).

At low Ca levels, the PTH is released from epithelial cells of the parathyroid gland and is immediately transported to its target cells via the bloodstream. PTH prevents hypocalcemia by rapid metabolization of crystalline structures in the bone. In the proximal tubule of the kidney, PTH inhibits the absorption of phosphate and increases its renal excretion. In the loop of Henle and in the distal tubule of the kidney, PTH leads to an increased absorption of Ca. As a result, the Ca mobilized from bones is retained in the organism (24).

Another important player is calcitriol, which is synthesized from provitamin 7-dehydrocholesterol. Upon exposure to ultraviolet light, 7-dehydrocholesterol becomes cholecalciferol, the so-called vitamin D3 (calciol) within two hydroxylation processes in the liver and kidney. As a result, the active hormone 1,25 (OH) 2-cholecalciferol is produced. PTH increases the activity of renal 1-alpha-hydroxylase and promotes the formation of calcitriol. The main target of calcitriol is the intestine, but effects have also been proven in the kidneys (25). Calcitriol binds to specific intracellular receptors resulting

in the opening of Ca channels in the intestinal brush border membrane. Ca-ions are bound to calbindin inside the cell and transported to the basolateral membrane in their biologically inactive state. The Na^{+}/Ca^{2+} -antiporter exchanges Ca- for Na-ions, in the blood. This results in an influx of Ca from the intestine into the plasma and in suppression of PTH secretion. Therefore, calcitriol inhibits the osteoclasts and promotes osteoblast activity (25). The bone matrix increases and is calcified by the incoming Ca. The peptide hormone calcitonin is produced in the C cells of the thyroid, parathyroid and thymus. It is released when the plasma Ca level is increased to > 2.6mmol/l, whereupon Ca is stored in the skeleton. Accordingly, calcitonin is an antagonist of PTH in terms of Ca metabolism in the bone. In the kidney, however, PTH and calcitonin act synergistically. Both hormones lead to increased phosphate excretion (phosphaturia) and decreased Ca excretion in the proximal tubule of Henle's loop. Therapeutically, it is used to suppress pathologically stimulated osteoclast activity and thus promote the calcification of the skeleton (25).

1.4 Magnesium homeostasis

Magnesium (Mg) is a mineral abundant in the human body. In detail, an adult body contains about 25g of Mg and 50-60% is stored in the bones, and only less than 1% is found in the serum. In general, serum levels are tightly regulated and range from 0.75 to 0.95 millimoles (mmol)/L. Mg is an important cofactor in more than 300 enzymatic systems and is involved in protein synthesis, muscle and nerve function, blood glucose control, oxidative phosphorylation, glycolysis, bone development, and blood pressure regulation (26). It also plays a role in the active transport of Ca ions across the cell membrane. This transport process is responsible for the conduction of nerve impulses and, further, regulates muscle contraction and normal heart rhythm. Hypomagnesemia develops when Mg levels are lower than 0.75 mmol/L and can result in disturbances of all the aforementioned functions in various types of severity. The regulation of Mg homeostasis is mainly performed by the kidney. Approximately, 120mg of Mg is excreted in the urine per day. Mg reabsorption in the kidney is hormonally regulated by PTH, vitamin D, and calcitonin. In hypomagnesemia, urinary excretion decreases to counteract Mg loss (27). In addition, PTH ensures the release of Mg from bone during hypomagnesemia and an increase in absorption in intestine (28).

1.5 Osteoporosis

1.5.1 Definition

In 2001, the NIH Consensus Development Panel on Osteoporosis defined osteoporosis as a systemic skeletal disease characterized by inadequate bone strength, which makes patients prone to an increased risk of fractures (29). Bone strength primarily reflects the correlation between bone density and bone quality. According to the WHO, the definition of decreased bone density is a T-value of -2,5 (29).

1.5.2 Epidemiology

Osteoporosis is the most common bone metabolism disease and affects around 370,000 women and 90,000 men, according to estimates by experts in Austria (30). The ratio of women to men is therefore around 4:1. About one third of all postmenopausal women and two thirds of all women over the age of 80 suffer from osteoporosis. The number of femoral neck fractures and vertebral body fractures steadily increases and will continue to rise without preventive countermeasures. The consequences of an osteoporotic fracture should not be underestimated, it is associated with a 2-5 times higher mortality within the first year compared to a healthy individual at the same age (31).

1.5.3 Types of Osteoporosis

A general distinction is made between primary and secondary osteoporosis, with the primary occurring far more frequently (32).

Primary osteoporosis: This type includes post-menopausal osteoporosis and senile osteoporosis. The decreased bioavailability of estrogen during post-menopause leads to less active osteoblasts and more active osteoclasts (high turnover). Accordingly, trabecular perforations and net absorption increases. Since the remodeling activity is higher in the trabecular bone than in the cortex, trabecular bone, such as the vertebral bodies and the pelvis, are more severely affected. Morphologically, a reduction in bone mass can only be seen in an X-ray, after a reduction of more than 30% in bone density. At the beginning, the least stressed trabeculae are resorbed and the cortex is thinned out, especially on the endosteal surface (33).

Senile osteoporosis mainly affects men and women equally, starting at the age of 65. Pathogenetically, osteoblast activity reduces (low turnover) in combination with a slight secondary hyperparathyroidism. Downscaled kidney function results in less Ca, which is available and the parathyroid glands are highly activated in a counteracting manner. Radiologically, a lightening of the entire skeleton is observable, unlike post-menopausal osteoporosis, where the trunk skeleton is mainly affected (33).

Secondary osteoporosis:

In contrast to primary osteoporosis, secondary osteoporosis is caused by another disease or treatment and is not congenital. There are many possible causes, including hypogonadism, hypercortisolism, primary hyperparathyroidism, severe renal insufficiency, malassimilation, type I diabetes mellitus, anti-epileptic therapy and anorexia (27,30). In the case of steroid osteoporosis, the steroids directly inhibit the protein synthesis of the osteoblasts. Depending on the extent to which protein synthesis by osteoblasts is suppressed, more or less pronounced osteoporosis develops. In steroid therapy or hypercortisolism (Cushing's disease), this mechanism is responsible for osteoporosis. The bone resorption via osteoclast activity is not influenced. The changes are particularly marked in the vertebral bodies, comparable to post-menopausal osteoporosis (27,33).

Low Magnesium and osteoporosis:

For many years Ca and VitD have been the master focus in the pathogenesis of osteoporosis and furthermore as additive dietary supplements for prevention (26). Overall Mg plays a key role as well and is an essential micronutrient with a variety of regulatory, structural, and metabolic functions. A significant association has been found between bone density and Mg intake. Over time, inadequate dietary Mg intake, for instance in a western diet consisting mainly of highly processed food low in micronutrients, will lead to hypomagnesaemia (34). Compensatory Mg is mobilised from the bone surface. The low Mg intake results in delayed bone differentiation and calcification, which overall negatively affects bone stiffness (35).

1.6 Fractures

1.6.1 Fracture classification

A fracture is an incomplete or complete interruption of bone continuity, which can emerge traumatically, through permanent stress or due to a pathological bone structure. Traumatic fractures are induced by mechanical, mostly shock-like loading, whereas fatigue fractures occur after prolonged mechanical overuse of the bone. Pathological fractures are a result of primary tumours, metastases or osteoporosis. Typical for pathological fractures is that they most likely appear without adequate trauma. Further subdivisions are closed / open fractures, the number of fragments and the fracture line course. The latter can be further divided in transverse, longitudinal, oblique, spiral, T or Y fracture. The fracture line course is also described by the dislocation of a fracture when the fragments are displaced relative to one another (16). Depending on the type of force and muscle pull, there are 6 forms of dislocation (Figure 1).

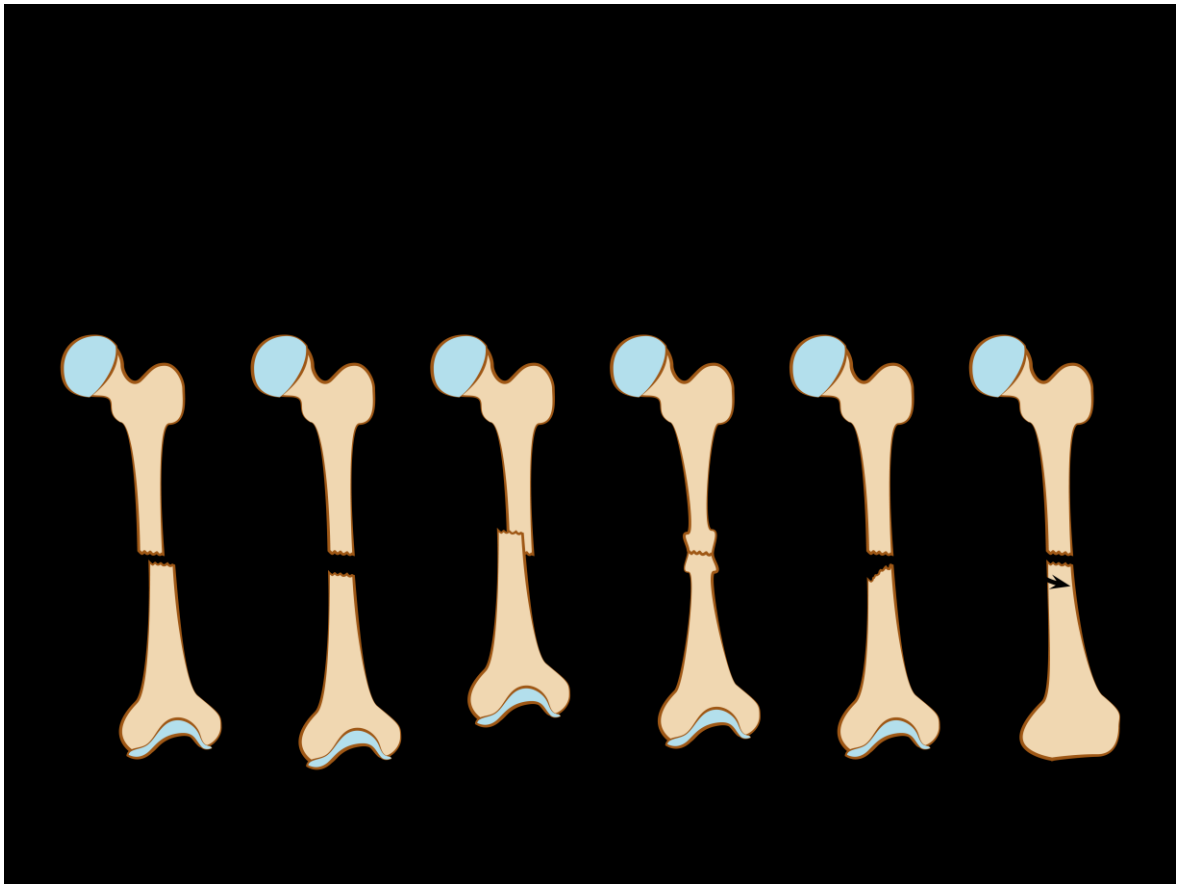

Figure 1: Illustration of the six different forms of dislocation that can occur in the case of a bone fracture. Reference: Own illustration inspired by (36)

1.6.2 Fracture healing

Bone fractures classically heal directly or indirectly, depending on the biomechanical properties of the particular fracture. Indirect bone healing (secondary bone healing) represents the natural healing process, whereas primary bone healing (direct bone healing) is owed to surgical procedures, using plates and screws. During direct bone healing, the narrow fracture gap (<1mm) is immediately filled with lamellar bone. However indirect healing is based on a cartilaginous preliminary stage (37).

Bone fractures lead to destruction of bone cells and bone matrix, disruption of endosteum and periosteum as well as the formation of a localised haematoma in the fracture zone. The hematoma clot in between the fracture ends, activates platelets, which release biologically active factors such as vascular endothelial growth factor (VEGF), platelet derived growth factor (PDGF), tumor growth factor-beta (TGF-β), insulin like growth factor (IGF-1) or precursor epidermal growth factor (PEGF). Initially the inflammatory phase starts. At the beginning neutrophils migrate into the tissue, phagocytize dead cells and further release chemotactic substances (37). Later on macrophages and monocytes are also found in the injured tissue, removing dead tissue and initiate immunological processes for wound healing. Locally other inflammation mediators such as interleukin-1 (IL-1), interleukin-6 (IL-6), interleukin-8 (IL-8) and tumour necrosis factor-α (TNF-α) are released (38). Especially in the initial phase the unspecific immune response plays a key role in interacting with osteoclasts and osteoblasts, via cell immigration and their release of cytokines and other inflammation mediators. These mediators influence the participating cells which built-up and breakdown bone substance. A special role has TGF-ß, which includes bone morphogenetic proteins (BMP). BMP are growth factors and a subgroup of cytokines, differed into 20 subtypes. Via extracellular serine-threonine-kinase signalling pathways they influence the intracellular SMAD-signal pathway. SMAD proteins act increasing or decreasing on gene transcription in the cell nucleus. This mechanism is needed for osteogenic differentiation of mesenchymal cells, pre- and postnatal, creating our musculoskeletal system. Furthermore progenitor cells, located in the endosteum, periosteum and soft tissues, differentiate into osteoblasts and chondrocytes for bone healing via SMAD-signal influence (37). After three weeks the initial hematoma is increasingly replaced with cartilage and bone tissue (38). Firstly chondrocytes dominate and soft callus is created. Within time the soft callus is gradually transformed into hard callus by osteoblasts and osteoclasts. As a result, the former fracture zone gains stability and pain in this area is decreased. In the final step the fibrous bone is broken down and

replaced by the original lamellar structure of the bone. For the first time a visible radiological consolidation can be demonstrated, at this time point. Nevertheless, the complete bone remodeling process can take years to complete (16).

1.6.3 Fracture healing in osteoporosis

As described above, the formation of new bone matrix is a complex biological process with many small individual steps. As a result, some difficulties arise in the osteoporotic, metabolically disturbed bone. In post-menopausal osteoporosis type I, estrogen deficiency impairs the early and late phase of fracture healing in callus formation, bone mineral density and mechanical properties. Although impaired osteoporotic fracture healing is multi-factorial, Neidlinger-Wilke et al. showed that low sensitivity of osteoblasts might be a reason for the insufficient mechanical signalling in osteoblasts (39). Furthermore, decreased mesenchymal stem cell count and reduced angiogenesis might cause impaired fracture healing (40,41).

The effect of aging in osteoporotic fracture healing demonstrated delays in osteoblast and chondrocyte differentiation. In comparison, juvenile mice are able to generate greater numbers of osteocalcin-expressing osteoblasts and Col-II-expressing chondrocytes. This initiates more rapid cell proliferation and more resilient periosteal reaction (8). During the late phase of fracture repair, there is less trabecular bone formation in the callus area of elderly mice. The bone remodeling process is hence considerably slower than in younger mice. Although fractures do heal in the elderly, prolonged responses suggest deficits in mesenchymal stem cell activity. Clinically these findings engendered trying rejuvenation via bone marrow transplantation. The experiment showed better, swifter callus remodeling, more resilient callus formation and enhanced fracture repair in aged animals. Therefrom deduced, independent functionality of both immunological cells and mesenchymal stem cells is necessary for sufficient healing (40,42).

Another point which must be taken into account are the injured blood vessels, surrounding the fracture zone. The result is an ischemic microenvironment around the site of fracture. For repair angiogenesis and vasculogenesis is promoted by anabolic factors for instance vascular endothelial growth factor (VEGF) and hypoxia inducible factor-1-alpha (HIF-1 α). In the elderly the expression of obligate anabolic factors is suppressed. The combination of prolonged revascularization, minimal nutrient exchange and decreased oxygen supply results in cell death in common with delayed chondroblast and osteoblast

cell activity (40,43). Furthermore matrix metalloproteinase (MMP) activity lessens with age. Normally, MMP splits peptide bonds in proteins, which is necessary for degradation of cartilaginous matrixes. The MMP malfunction disturbs vascular invasion during ossification and retards degradation of cartilaginous matrix in the elderly (44).

1.7 Fracture treatment principles

A basic distinction is made in the therapy of bone fractures between conservative and operative approach. Conservative treatment is preferably used for undislocated fractures (except for undislocated, load-bearing bone fractures), for fractures in childhood and for patient showing contraindications like an uncontrollable bleeding disorder. Indications for operative care are a dislocation of bone fragments, form unstable, multi-fragmentary, joint and extensive tissue fractures (36).

1.7.1 Surgical fracture treatment

Patients only undergo surgical therapy if there is a strict indication. The approved indications include:

- Open fractures
- Closed fractures with grave accompanying injuries
- Dislocated joint fractures
- Fractures in polytrauma patients
- Avulsion fractures
- Fractures with pronounced dislocation or rotational misalignment

Relative indications apply to a large number of other types of fractures where osteosynthesis helps to avoid immobilization. A distinction is made between general and local contraindications. General contraindications apply to the entire organism and local ones to the operating area itself. During osteosynthesis, bone fragments are stably fixed together with the help of metal plates, metal screws and intramedullary nails (36). These are fixation elements made from tissue-friendly materials of various shapes, stiffness and dimensions. Osteosynthesis creates a balance between the stability required for fracture healing and the local biology in order to avoid healing disorders.

Three basic principles are followed with osteosynthesis:

- Repositioning
- Retention (via implant)
- Rehabilitation

There are two different approaches to surgical fracture treatment. Direct / primary fracture healing: During surgery fractures are repositioned and the fracture ends are compressed directly against one another, fixed and stabilized. Through this method healing occurs without callus formation.
Indirect / secondary healing: Secondary fracture healing just uses indirect repositioning of the fragments to ensure vascular supply in the area of trauma. Precise anatomical repositioning is refrained to obtain optimal blood flow to the bone, especially in case of complex, comminute fractures. It is merely paid attention to restore the axis, rotation and length of the bone as precisely as possible with a plate or a nail. Only small incisions are made into the skin to protect soft tissue near the fracture and warrant good healing conditions. The healing then takes places via enchondral bone healing with callus formation (36,45).

1.7.2 Materials for fracture stabilization

The gold standard today continues to be implants made of non-absorbable materials such as stainless steel, titanium or cobalt-chromium. Metallic materials have become established because they exhibit high mechanical strength, stiffness, excellent fatigue properties and not to neglect are comparatively cheap in their production compared to biodegradable implants (9,46). Nevertheless several disadvantages of metallic materials are described including corrosion, with subsequent precipitation of potentially toxic ions, inflammatory processes, allergic reaction, encapsulation and stress shielding. Steel implants may lead to encapsulation in connective tissue, increasing the risk of infections and implant loosening. Titanium implants have a better allergic compatibility, but cause more material fractures in second surgery for implant removal (46). The indication for implant removal should be kept very strict, especially in osteoporotic bone, even after fracture healing has been completed. The risk of refracture and the risk of re-anaesthesia must be explained in detail to ensure satisfactory healthcare (24).

1.7.3 Magnesium based alloys

Due to biodegradability and unnecessary removal surgery, Mg alloys have gained major attention in trauma research and osteoporotic fracture treatment. However, the variable degradation rate of different Mg alloys needs intensive research to develop an implant material showing a satisfactory degradation rate. Rapid dissolving bioresorbable implants do not allow sufficient fracture healing and damage bone tissue by swift corrosion and release of large amounts of hydrogen gas. Several Mg alloy compositions with different coatings and fabrication methods have been tested *in vitro* and *in vivo* (47).

In recent reviews by Zhao et al. and Luo et al. a wide variety of alloys, surface treatments and local and systemic reactions were illustrated in an overview (48,49).
The combination of Mg-Zinc (Mg-Zn) achieved a 58% higher bending stability than pure magnesium and alloys of Mg-Ca, Mg-Silver (Mg-Ag) showed a significant improvement in tensile strength (50–52). The triple combinations of Mg-Zn-Ag, Mg-Zn-Ca additionally enhanced the hardness and retarded the corrosion rate (50,53). A complete absence of gas formation was not achieved in any study.

Grün et al. compared the degradation behaviour and osseointegration of an implant containing Mg, Zn and Ca (ZX00) in a small and large growing animal model. The degradation rate between the two growing animal models did not differ significantly and both showed a slow and homogeneous degradation rate. Despite the low degradation rate (estimated completed resorption after 2 years), increased gas formation was observed, but without visible impairment of bone formation. The conclusion of the study was that small animal models are sufficiently suitable for further investigations to provide information about the degradation rate and preliminary data on bone formation (54).

In another study, Holweg et al. modified the Zn content of ZX10 to 0.45 wt.% and the Ca^{2+} content to 0.45 wt.%, achieving a slower degradation rate and improved mechanical strength, *in vitro*. The new compound called ZX00 was tested *in vivo* in a large growing animal model. One group was osteotomised and screwed and the second group was screwed only. After 12 weeks, all ZX00 osteotomies were found to be completely consolidated with no adverse side effects (55).

Lately Herber et al. published a study showing the mid-term results of ZX00 fixation after medial malleolar fracture in human. Twenty patients were included. Seventeen patients received additional fixation of the distal fibula or the dorsal tibial fragment with conventional titanium implants. After 6 and 12 months visual analogue scale for pain and presence of complications were evaluated. No patient was showing pain, complications, shoe conflict or misalignement after a 12 months. In the plane radiographs, performed one year after implantation, the Mg screw heads could not be detected, suggesting satisfying degradation of the majority of the screw head without adverse reactions (56).

1.8 Biodegradable Mg-based implants

1.8.1 Degradation behaviour of Mg

Back in the 19th century, researchers like Edward Huse observed that pure Mg corroded rapidly *in vitro*, even at normal physiological pH (1). Pure Mg corrodes at around 10.5-210mm per year under physiological conditions (equivalent to 3% NaCl solution). Corrosion is additionally accelerated in an acidic environment (inflammation) and slowed down in a basic environment (57). Myrissa et al. compared *in vitro* and *in vivo* degradation of pure Mg and Mg alloys. It was demonstrated that *in vivo* and *in vitro* results were only comparable to a limited extent due to various influencing factors, especially in terms of corrosion duration (Table1.) (47).

Table 1: *In vivo* and *in vitro* influencing factors. Reference: (58)

in vivo	***in vitro***
tissue pH	solution pH
vascularisation of the peri-implant tissue	solution temperature
chloride content	type of solution
type of organism	degradation behaviour of the solution
localisation of the implant	dynamic vs. static

1.8.2 Why using lithium

Lithium (Li) has been the gold standard in the treatment of bipolar disorder in psychiatry for years (59). Only recently, a completely different speciality, orthopedics and traumatology, realized the potential of this chemical element (32,60–64).

In general, appropriate fracture treatment fails in up to 10% (60). Another major problem with osteosynthesis is the local syndrome of bone destruction e.g. peri-implant osteolysis (PIO). Osteoclast activation plays a crucial role in PIO. Recent research of Pan et al. has shown that Li is capable of inhibiting osteoclastogenesis and proinflammatory cytokine release *in vitro*. They created a lithium-calcium-silicate (LCS) bioceramic to appraise the effect on RANKL-induced osteoclastogenesis *in vitro* and titanium particle-induced osteolysis *in vivo*. The results were promising and demonstrated the inhibition of RANKL-induced osteoclastogenesis through suppression of NF-kB signalling pathway, in a dose-dependent manner (61). Another study aimed to fabricate a Li-doped Ca-phosphate scaffold (LiCPP) to assess degradation behaviour, biocompatibility and osteogenesis *in vivo*. To evaluate the osteogenic potential, twenty adult male rabbits underwent implantation of LiCPP scaffolds. In general, CPP is insufficient to induce osteogenesis, however, LiCPP was beneficial for cell proliferation and attachment. *In vitro* studies revealed that the LiCPP scaffold co-cultured with MG63 osteosarcoma cells increased the Ca-phosphate deposition and bone specific ALP expression (62). Luo Y et al. used hydroxyapatite (HA) containing Li. HA alone is brittle and does not promote osteoinduction and vascularization although it possesses similar mineral components to bone. The incorporation of Li did not significantly change the degradation rate of the scaffold, but attained higher compress mechanical strength. Bone regeneration and new bone formation were significantly increased in this *in vivo* study (rabbit model). However, the anticipated angiogenic effect could not be observed (63). Another research group doped mesoporous silica nanospheres (MSN) with Li. In the combined material the degradability was significantly increased compared solely MSN. They observed enhanced ALP activity and improved osteogenesis-related genes (e.g. Runx2) in rat bone marrow stromal cells (32).

Taken together, these findings suggest that Li may be beneficial to enhance osteogenesis, suppress osteolysis and improve mechanical strength (32,33,60–65).

2 Hypothesis and aims of the study

The success of endosseous implants is highly predictable in patients showing normal bone status, but may be impaired in patients with osteoporosis. Mg is an interesting candidate for osteoporotic surgical fracture treatment because it plays a key role in osteoporosis prevention, has suitable mechanical properties and the ability to degrade over a certain period of time (7,10,51,53,54,57,66). Moreover studies have shown that Mg ions, which are released during the degradation of Mg-based materials are subsequently stored in the cortical bone and strengthen the weak osteoporotic bone (4,8,9). Previous results demonstrated beneficial effects of Li including enhanced osteogenesis, suppression of osteolysis and improved mechanical strength (32,33,60–65).

Accordingly, a Mg-4Li-1Ca alloy (LX41) was developed and investigated in an established juvenile, healthy animal model regarding biocompatibility and degradation behaviour. We compared it to another Mg-based alloy (Mg-Zn-Ca; designated as ZX00), which has already been used in pre-clinical and clinical trials. Based on preliminary, unpublished data from our group, we can demonstrate that ZX00 degradation is enhanced in a ovariectomy-induced osteoporotic rat model. Since previous studies demonstrated improved mechanical strength due to the incorporation of Li, we hypothesized that LX41 may be applicable in osteoporotic rats and we therefore expected a slower degradation, which should already be evident in the established juvenile, healthy animal.

Based on the preliminary studies with ZX00 in juvenile healthy rats, we hypothesized that:

(i) the degradation rate of LX41 is slower than ZX00
(ii) the degradation rate is homogenous, leading to adequate gas formation and osseointegration

To test our hypotheses, LX41 pins were transcortically implanted into the metaphyseal area of the proximal tibiae in juvenile, healthy rats. The most important parameters including implant volume, implant surface and gas volume were investigated using *in vivo* low-medium resolution micro-computed tomography, to assess the degradation behaviour of the LX41 alloy and indirectly compare it to ZX00 (previously analysed in another diploma thesis by Lisa Paar, 2021). Additionally, histological analysis LX41 and ZX00 was assessed regarding osseous integration and gas formation.

3 Material and Methods

3.1 Ethical statement

Small animal studies were confirmed by the Austrian Federal Ministry for Science and Research and in compliance with the guidelines on accommodation and care of animals formulated by the European Convention for the Protection of Vertebrate Animals used for Experimental and Other Scientific Purposes (GZ number: BMWFW66.010/0124-WF/V/3b/2015). All animal experiments followed the 3R principles (replace, reduce and refine) to minimize suffering.

3.2 Material development

For the pins, a ternary Mg-Li-Ca cast alloy with 0.04wt% Li and 0.01%wt Ca was synthesized (designated as LX41). Firstly pure Mg (99.95%) and Mg-30Ca master alloy were melted in a graphite crucible. Subsequently Mg-14Li master alloy was added at a temperature of 720 °C under constant, vigorous stirring. The melted material was then poured into a copper mold coated with a thin layer of boron nitride / alumina. Before hot rolling at 300 °C the samples were cut from the ingot and received homogenization treatment at 350 °C for 2h. In the last step samples were cut from the rolled plate and mechanically polished with diamond paste and chemically etched with 10% Nital solution for 25-30s.

3.3 Animals and surgery

Four weeks old, female Sprague Dawley rats (n = 7) were purchased from Janvier Labs (Saint Berthevin, France) and accommodated on normal chow for the entire study. A conventional facility with free access to water and food and a 12-hour light/dark cycle was provided for all rats. At an age of six weeks, seven Sprague Dawley rats underwent surgery. The cylindrical LX41 implants were inserted bilaterally, transcortically and proximally into the metaphysis of the tibiae (two implants per rat; 14 implants in total).

The same surgical intervention was performed on two further Sprague Dawley rats but without an implant, thereby presenting as sham controls.

3.4 Anaesthesia

For general anaesthesia volatile isoflurane (Forane®, Abbot AG, Baar, Switzerland) was administered. Beforehand, a subcutaneous combined sedation including Fentanyl (20 µg kg−1 Fentanyl®, Janssen-Cilag GmbH, Neuss, Germany), Midazolam (400 µg kg−1 Midazolam Delta®, DeltaSelect GmbH, Dreieich, Germany) and Medetomidine (200 µg kg−1 Domitor®, Pfizer Corporation Austria GmbH, Vienna, Austria) was administered.

3.5 Transcortical implantation

Preoperative preparation included shaving, disinfection with alcohol pads and drying of both hind legs. A 1-2cm long skin incision was made medial over the proximal lateral tibial metaphysis and the soft tissue was exposed. The bicortical implantation bed was prepared with a 1.55mm drill showing an ascending diameter (Synthes, Paoli, PA, USA). A low rotational speed of 200 rpm was used for drilling. To minimize frictional heat and thermal necrosis abundant physiological saline irrigation was utilized using a syringe. Through gentle tapping the cylindrical implant (l=8 mm, d= 1.6 mm) was positioned, resulting in a uniform press fit. Correct transcortical placement was warranted, the operating field was rinsed adequately with physiological saline solution and the wound was stitched up. To ensure postoperative analgesia all Sprague Dawley rats received 200 mg kg-1 Caprofen (Rimadyl, Pfizer Corporation, Vienna, Austria). Caprofen was injected subcutaneously on the day of operation. Analgesia was perpetuated by administration of 60 mg Piritramid (Dipidolor; Janssen-Cilag GmbH, Neuss, Germany) in 40 ml 5% glucose added to 500 ml drinking water for the first postoperative week. Postoperatively, the Sprague Dawley rats were permitted to move unrestrained in their cages and unrestricted weight bearing. Throughout the whole study period daily clinical observation was performed.

3.6 Euthanasia

Euthanasia was performed twenty-four weeks after transcortical implantation with 25 mg sodium thiopental (Thiopental® Sandoz, Sandoz GmbH, Kundl, Austria) by injection into the cardiac ventricle leading to instantaneous cardiac arrest. All tibiae were explanted and stored at -80 °C for further investigation.

3.7 In vivo low-medium resolution micro-computed tomography (µCT)

In vivo µCT(Siemens Inveon µCT device) scans were rendered 2, 12, 18 and 24 weeks after surgical implantation or sham surgery (n = 9) at a resolution of 56 µm per voxel. The raw scan data were converted into DICOM format and imported into the medical image processing software Mimics (Version 23.0, Materialise, Leuven, Belgium). Via three-dimensional (3D) morphometric analysis implant volume, surface area, gas and bone volume were assessed. At each µCT time point, animal weight was monitored to record weight deviations.

3.8 Quantification of implant degradation parameters

Quantification of the implant degradation behaviour was performed via Mimics Software, version 23.0. Each tibia was evaluated individually via function “Image-Reslice Images”. Image-Reslice Images illustrates the implant in all three planes and in all layers. In order to demonstrate the implant, the transversal and longitudinal axes of the implant were used as main indicators for editing (Figure 2a).

3.8.1 Quantification of implant volume and surface

Via function „Segment - New Mask“ a threshold of 220 to 3071 Hounsfield Units (HU) was placed on the images to separate bone from implant (Figure 2b). As the aforementioned thresholds of Hounsfield Units did not comprise bone and implant in all µCT images, the threshold values of Hounsfield Units had to be adaped individually. Via function „Segment - Split Mask“ µCT images could be divided in two masks, the rats bone and the Mg implant (Figure 2c). After separation of the two masks a manual post-

processing in all planes had to be fulfilled to correct the partially imprecise calculated parts. The correction ensured a precise calculation of the implant volume and surface values. A three-dimensional (3D) model of the implant was designed via function „Mask - Calculate Part“ and volume (in mm^3) and surface (in mm^2) values were analysed (Figure 6).

3.8.2 Quantification of gas volume

A second mask was created with “Segment-New Mask”, using -879 to -1024 Hounsfield Units, to quantify the generated hydrogen gas volume. For precise measurement of each entire gas volume the threshold values were modified individually. A 3D model of the gas volume was designed via the function „Mask – Calculate Part“ and subsequently the gas volume was calculated in mm^3 (Figure 2d).

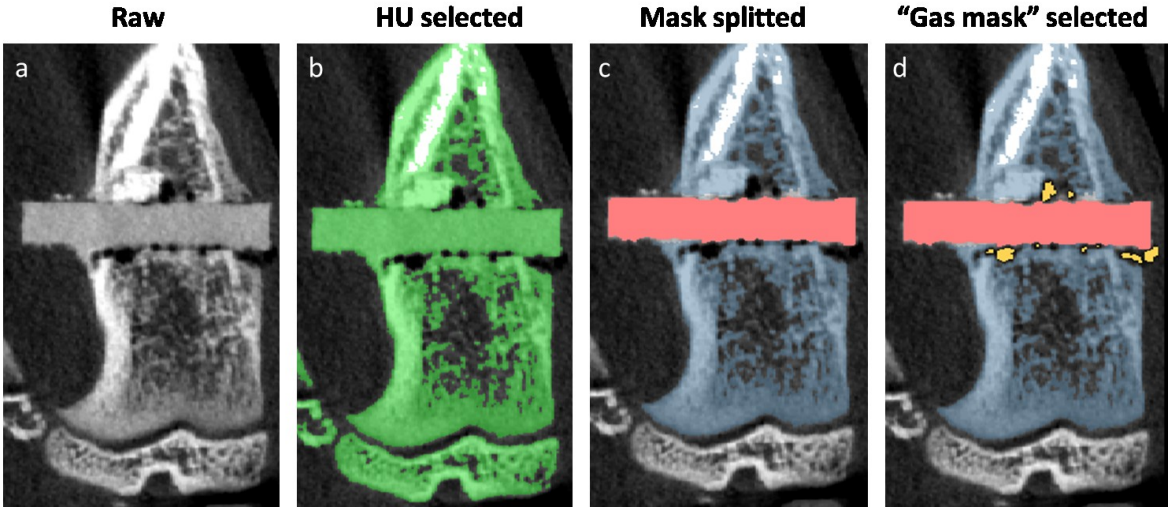

Figure 2: Segmentation of images obtained by *in vivo* low-medium resolution µCT. Scanswere performed immediately after pin implantation as well as 2, 12, 18 and 24 weeks afterwards. (a) The µCT image data underwent segmentation via gray value orientated region growing algorithm: For the quantification of implant volume and surface, as well as gas volume, µCT images were resliced and evaluated via Mimics Software Version 23.0. (b) Bone tissue and the LX41 implants show similar HU. (c) Therefore, individual pin and gas evolution segmentation was performed. (d) To quantify gas evolution a new mask (“Gas mask”) was added. The dark spots representing gas evolution nearby the implant were evaluated using the region growth function. Reference: Own illustration

3.8.3 Computation of the degradation rate

The degradation rate, DR_i, was determined similarly to previous studies (54):

$$DR_i = \frac{\Delta V_i}{\bar{S}_i \Delta t},$$

With i the observation time point, ΔV_i the volume change and $\bar{S}_i$ the average surface area between two observation time points Δt.

3.9 Histological evaluation of implant degradation

The removed tibiae were cut to the desired region and fixed in 100 % ethanol. The ethanol prevents further degradation of LX41 on the one hand and serves to preserve the tissue on the other. To ensure dehydration, the ethanol was changed daily for three days. This was followed by infiltration with Technovit 9100 resin (Kulzer GmbH, 63450 Hanau, Germany) according to the instructions for use and final embedding in the same resin. Undecalcified thin sections of the targeted regions were fabricated with a thickness of about 100 µm according to the Karl Donath method (67). The sections were stained with methylene blue, azure I, and basic fuchsin (68). The thin sections were transformed into digital images using a custom-built Olympus BX53 scanner system (OLYMPUS EUROPA SE & CO. KG, Hamburg, Germany).

3.10 Statistical analysis

Not all 14 implanted materials could be investigated, so that the number of samples was below 10. Nevertheless, all results are still given as mean ± standard deviation to make them comparable between all groups and to literature. Differences between groups and time points were assessed via two-way ANOVA using the Bonferroni's post-hoc test. A p-value < 0.05 was considered statistically significant.

4 Results

Seven four weeks old Sprague Dawley rats underwent bilateral and transcortical implantation into the proximal metaphysis of the left and right tibiae. For implantation, cylindrical LX41 pins (l=8 mm, d=1.6 mm) were used. Immediately after surgery low-medium resolution µCT scans were performed immediately after surgery (t0) as well as 2, 12, 18 and 24 weeks after implantation. Moreover histological evaluation of LX41 and ZX00 samples was performed (Figure 7).

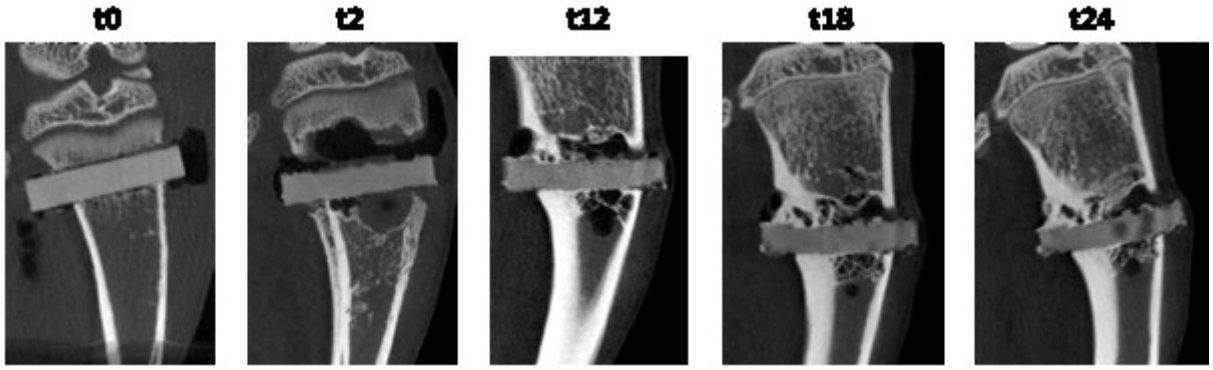

Figure 3: *In vivo* observation of LX41 degradation over 24 weeks via µCT imaging. Cylindrical LX41 pins were transcortically inserted into the proximal metaphysis of the right and left tibia of 4-weeks old Sprague Dawley rats. Degradation behaviour, bone growth and osseointegration were evaluated immediately after surgery (t0) as well as 2, 12, 18 and 24 weeks post implantation. Reference: Own illustration

4.1 Degradation behaviour of LX41 implants evaluated via calculation of implant volume and implant surface alteration compared to ZX00

Implant degradation behaviour was evaluated via calculation of volume differences of the implant in Mimics Software, Version 23.0. In total, 14 implants were measured at six different time points (time point 0, 2, 6, 12, 18 and 24). Due to the poor image quality of time points 6 and 12, they could not be analysed. The initial volume of the LX41 pins (time point 0) was measured with an average value of (15.67 mm^3±0.20 $mm^{3)}$. Therefore, we started with 0.72 mm^3 less mean volume than ZX00 with an initial volume of (16.39 mm^3±0.56 mm^3). Two weeks after implantation, we did not observe an increase in volume of LX41 when compared to ZX00. Eighteen weeks after implantation, the LX41 implant volume decreased to an average value of (9.78 mm^3± 0.58 mm^3). In comparison, the

implant volume of ZX00 was (14.69 mm^3± 0.734 mm^3) 18 weeks after implantation. After 24 weeks, all rats were sacrificed and the mean volume of LX41 implants reached (9.49 mm^3±0.91 mm^3), when compared to ZX00 with a volume of (13.93 mm^3±1.27 mm^3) *(69)*. On quantitative level, the mean volume loss until 24 weeks was 6.07 mm^3 for LX41 and 2.82 mm^3 for ZX00 pins. The relative analysis of implant volume loss over the entire study period revealed 37.60% for LX41 pins compared to 11.99% for ZX00 pins. Additionally, we calculated the degradation rate for LX41 pins and compared it to ZX00. Interestingly, the degradation rate of LX41 was almost two-fold higher (0.721 µm ±0.15 µm per day) in LX41 compared to ZX00 (0.34 µm ±0.10 µm per day) (69).

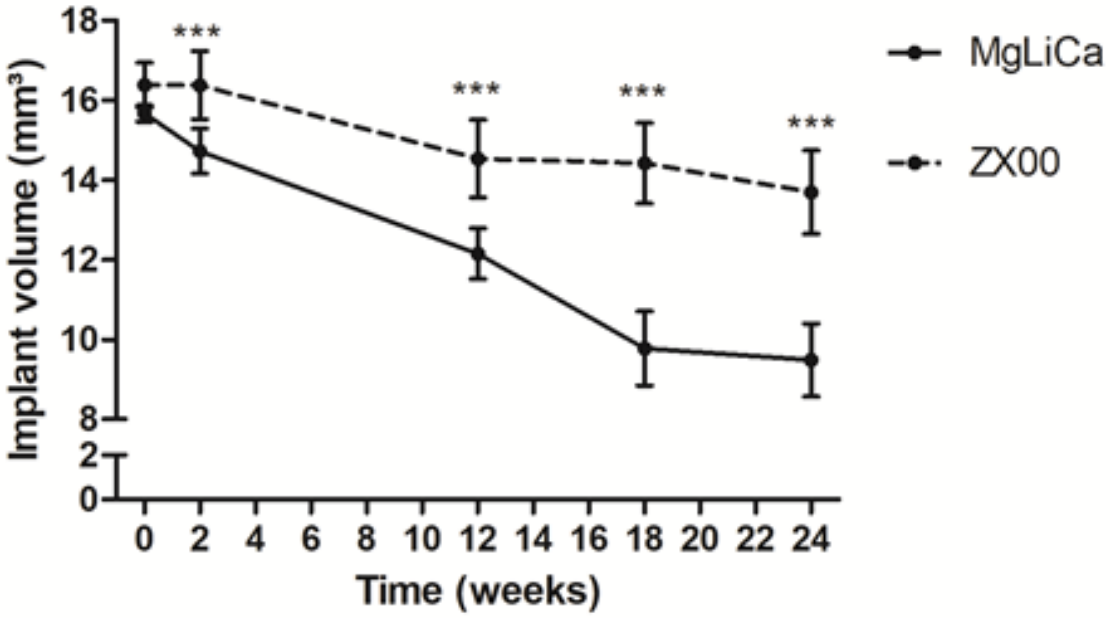

Figure 4: Comparison of implant volume alteration between LX41 and ZX00 over the entire study period of 24 weeks (ZX00 data was provided by Lisa Paar, accessible in the diploma thesis and adapted here to serve as internal reference) (69*)*. The different implant volume values were evaluated at five different time points (0, 2, 12, 18 and 24 weeks after implantation). Data is shown as mean ± standard deviation (SD). Reference: Own illustration

Immediately after implantation (time point 0), the average implant surface of LX41 and ZX00 implants measured almost the same with (47.43mm^2±1.27mm^2) for LX41 and (47.44 mm^2±1.89mm^2) for ZX00. Only marginal surface alterations could be observed in implant

surface value for LX41 and ZX00 pins after 2, 12 and 18 weeks. At the end of the study (t24) mean implant surface values of both materials differed significantly. LX41 implants decreased to (44.53 mm^2±4.22 mm^2), whereas in ZX00 an increase to (54.94 mm^2±5.65 mm^2) was evaluated (69).

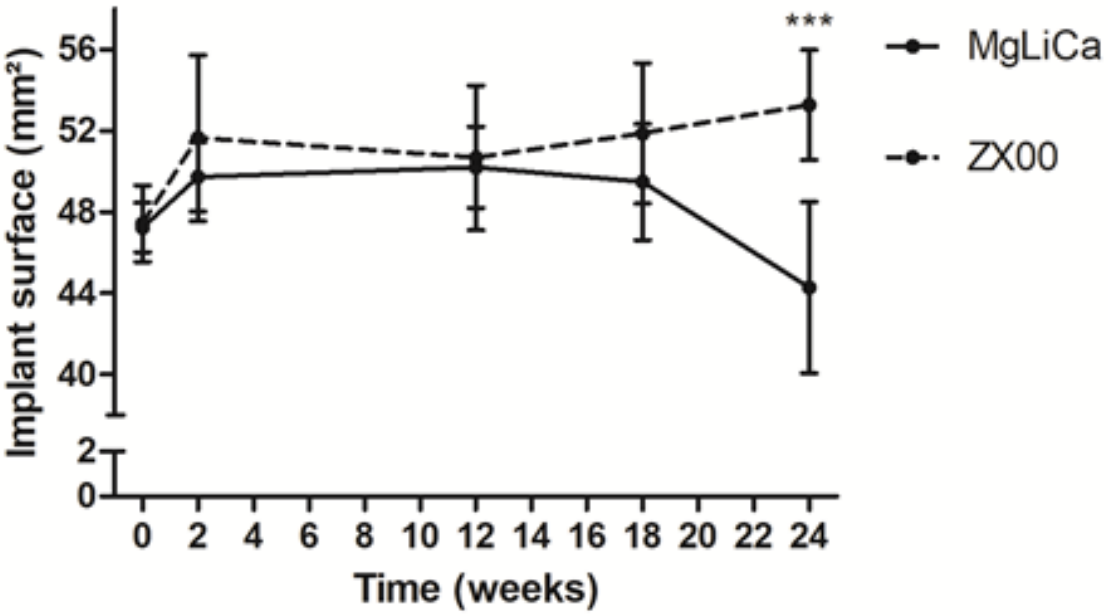

Figure 5: Comparison of implant surface alteration between LX41 and ZX00 over the entire study period of 24 weeks (data adapted from (69). The different implant surface values of LX41 and ZX00 implants were evaluated at five different time points (0, 2, 12, 18 and 24 weeks after implantation). Data is shown as mean ± standard deviation (SD). Reference: Own illustration

4.2 Evaluation of hydrogen gas formation in vicinity of LX41 implants compared to gas formation in ZX00 implants

During the degradation process of magnesium, hydrogen gas is released. The evaluation of hydrogen evolution over 24 weeks was performed via *in vivo* low-medium resolution µCT imaging. Subsequently three-dimensional reconstruction of LX41 implants and hydrogen gas pockets were performed by Mimics Software, version 23. Hydrogen gas volume was measured at four different time points (t2, t12, t18, t24) over an entire time period of 24 weeks, starting with the first measurement two weeks after surgery. At the starting point 0, air inclusions were observed occurring due to the implantation process and therefore not

measured. At time point 2 the mean value of hydrogen gas volume was significantly higher for LX41 implants measuring (15.72 mm^3±9.87 mm^3) and only (2.87 mm^3±3.47 mm^3) for ZX00 implants. This time point showed the highest hydrogen gas levels for LX41 and ZX00. In the further course of the study, gas evolution gradually reduced, reaching an average value of (2.19 mm^3±2.36 mm^3) at the end of the study (t24). Same was observed in ZX00 reaching an average value of only (1.58 mm^3±1.53 mm^3) 24 weeks after implantation (69).

a)

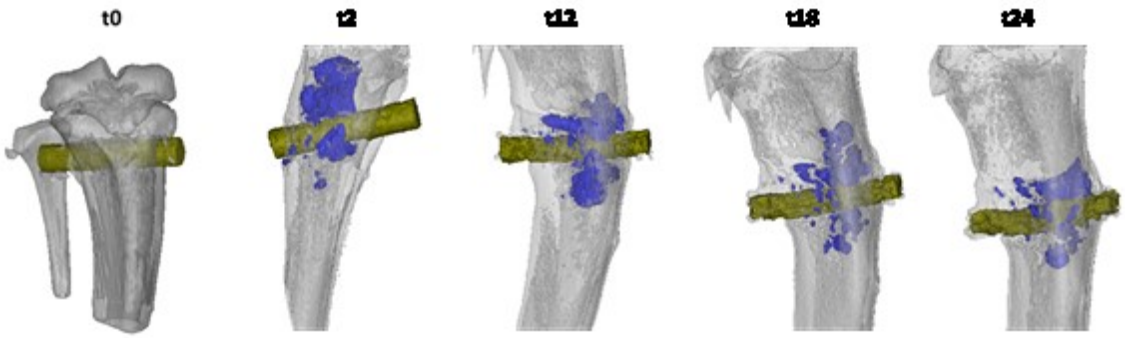

b)

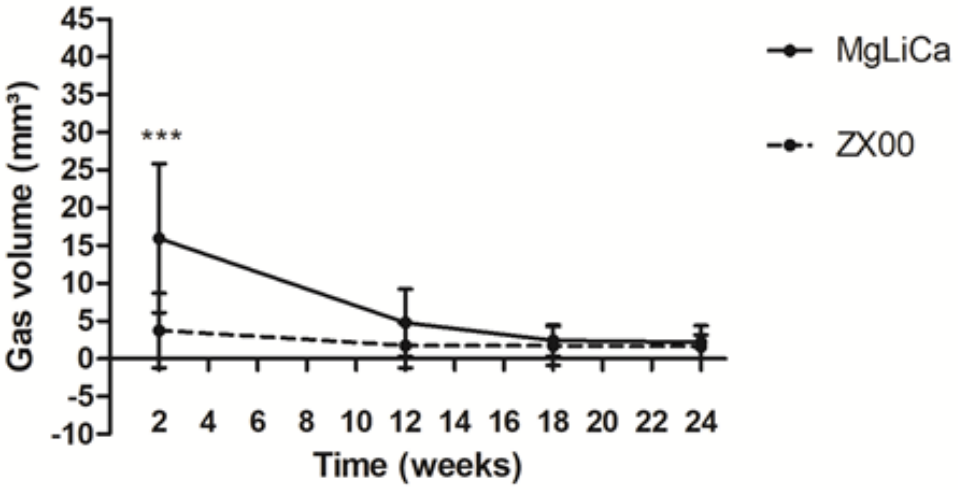

Figure 6a-b: a) For illustrative purposes, one LX41 pin was reconstructed three-dimensionally via Mimics 23.0. at the time points 0, 2, 12, 18 and 24 weeks after implantation.

b) Comparison of hydrogen gas evolution between LX41 and ZX00 over the entire study period of 24 weeks (data adapted from (69). Generated gas volume of LX41 and ZX00 implants were evaluated after bilateral transcortical implantation into the left and right tibia

of Sprague Dawley rats 2, 12, 18 and 24 weeks after implantation. Data is shown as mean ± standard deviation (SD). Reference: Own illustration

4.3 Histological evaluations of osseous integration and gas formation in LX41 pins and ZX00 implants

In order to evaluate bone-to-implant contact, bone morphology and any adverse events initiated by LX41 and ZX00 implantation, bones were excised 24 weeks after implantation, dehydrated and embedded in Technovit 9100 New. Region of interest was stained with Levai-Laczko (Figure 7-10). The overview showed an intact bone marrow cavity, despite the presence of gas bubbles (Figure 7). The gas bubbles contained light brown cell detritus, but there were no signs of any acute inflammatory reaction or granuloma formation present in the bone tissue. A newly formed bone layer surrounded the pin almost entirely in the bone tissue area. Particularly, at the pin tips, pin degradation could be observed as dark blue degradation clods. The partly visible grey striae were an artefact that occurred when cutting the samples and therefore have no significance for the histological evaluation.

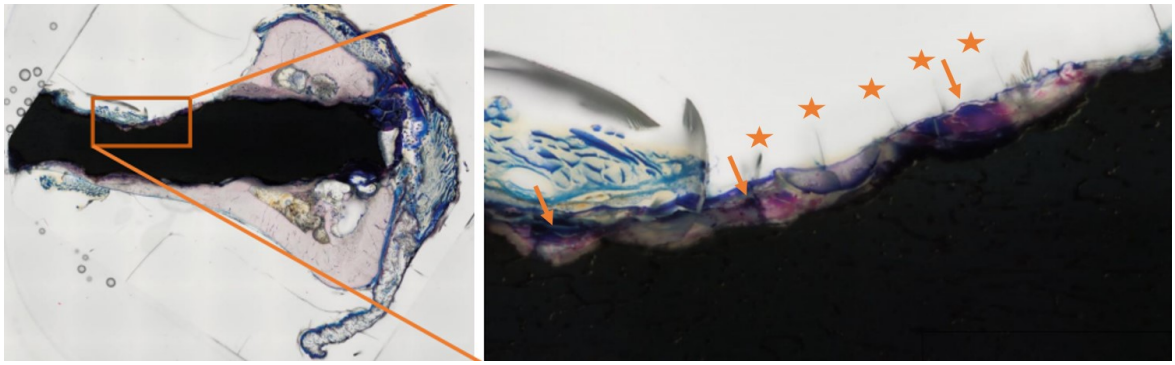

Figure 7: Qualitative histological analysis of the LX41 alloy in the proximal metaphysis of the tibia. Left: overview of the LX41 pin transcortically implanted into the tibia. Pinkish colour indicates bone, whereas blueish colour indicates connective tissue. Right: First region of interest at the bone-implant-interface. The orange arrows indicate larger cell nuclei; the orange asterisks highlight grey striae, which are an artefact of sample cutting. Reference: Own illustration

In the magnification of the first region of interest (left picture Figure 7; orange rectangle), we observed new dark pink coloured bone with larger cell nuclei in close proximity to the

LX41 pin (orange arrow). The grey striae marked with asterisks were an artefact of cutting the samples. Additionally, degradation products were observable at the interface to bone.

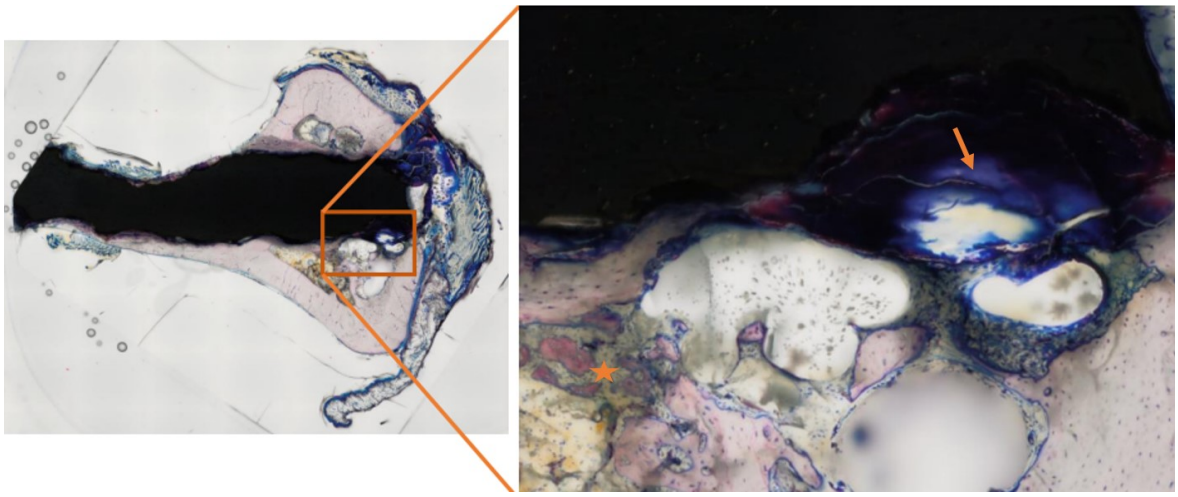

Figure 8: Second region of interest at the bone-implant-interface of LX41. Left: overview of the LX41 pin transcortically implanted into the tibia. Pinkish colour indicates bone, whereas blueish colour indicates connective tissue. Right: degradation products are highlighted with an orange arrow; the orange asterisk indicates newly formed bone. Reference: Own illustration

Gas bubbles with brown cell detritus were histologically visible adjacent to the pin. Dark blue degradation clods (orange arrow) were observable at the tip of the pin. Newly formed bone was observable lateral to the LX41 pin (pinkish area; orange asterisk). The light pink area further away of the pin contained small cell nuclei indicating older bone.

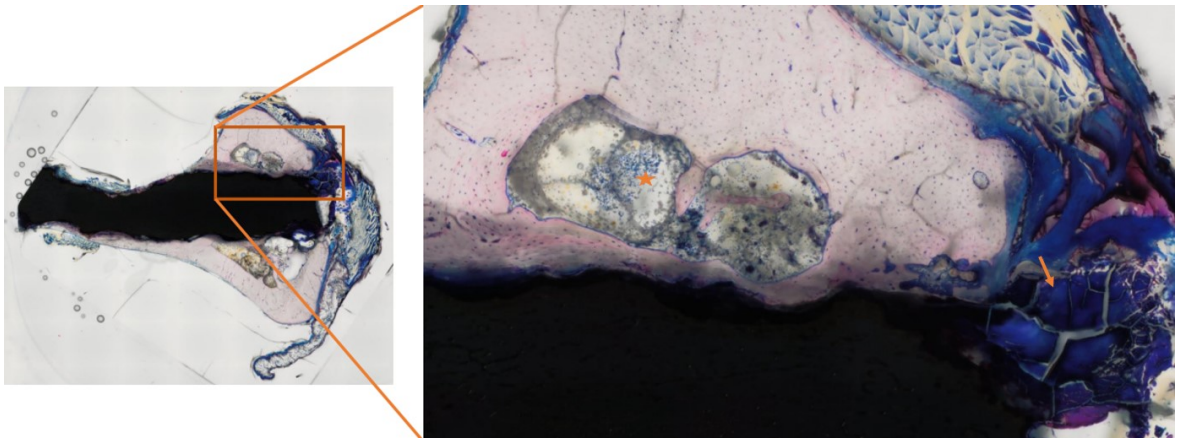

Figure 9: Third region of interest at the bone-implant-interface of LX41. Left: overview of the LX41 pin transcortically implanted into the tibia. Pinkish colour indicates bone, whereas blueish colour indicates connective tissue. Right: degradation products are highlighted with an orange arrow; cell detritus are marked with an orange asterisk. Reference: Own illustration

Dark blue crystalline degradation products were found at the pin end, which were released and broken down during the degradation process (orange arrow). Lateral to the pin, two gas bubbles were observable. Additionally, we highlighted blue erythrocytes and the light brown cell detritus inside the gas bubbles (orange asterisk). Moreover, the two gas bubbles were surrounded by old bone (light pinkish colour) in which small osteocytes were embedded.

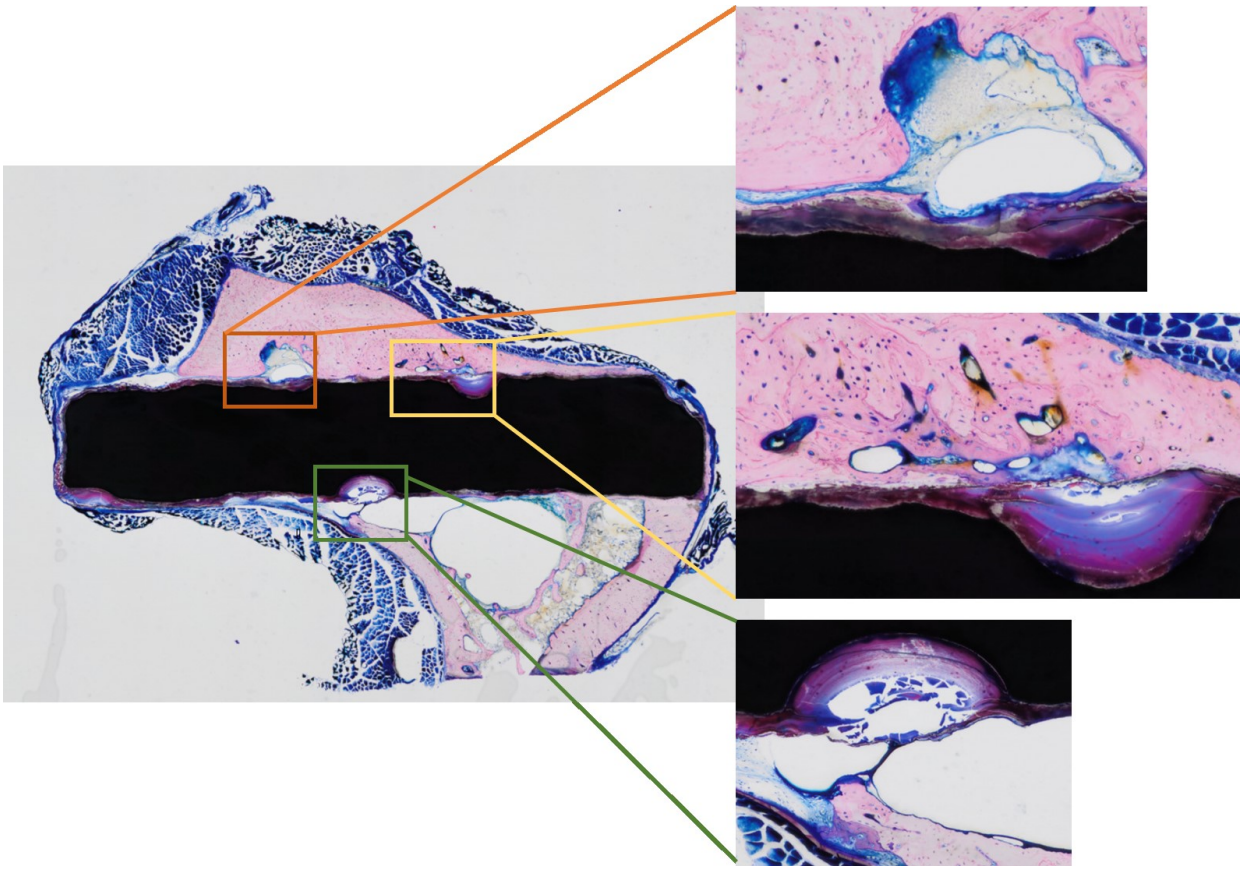

Figure 10: Three different regions of interest at the bone-implant-interface of ZX00. Left: overview of the ZX00 pin transcortically implanted into the tibia. Pinkish colour indicates bone, whereas blueish colour indicates connective tissue. Right: magnification of three different region of interest at the bone-to-implant interface. Reference: Own illustration

Qualitative histological staining of ZX00 pin revealed a good bone-to-implant contact indicating osseointegration (Figure 10). We observed gas bubbles filled with brownish cell detritus in the proximity of ZX00 (magnification; orange rectangle). Moreover, degradation lacunae containing pin degradation material (violet / bluish) was observable (magnification; yellow rectangle). Lateral to the pin, bigger cell nuclei were visible presenting newly formed bone. However, at the edge of the bone, smaller cell nuclei can be seen, indicating older bone. Additionally, degradation lacunae, which have already formed degradation clods were present (magnification; green rectangle). Next to the lacunae, a large gas bubble was observable, which contained no cell detritus, but a connective tissue wall.

5 Discussion

The aim of this study was to assess the degradation rate, gas formation and histological changes seen in the previously developed LX41 alloy. Furthermore, we directly compared the results with the already more established material ZX00 in terms of surface development, volume status and gas evolution. A previous *in vitro* study by Pan et al. showed that Li, as an alloying element, is capable of inhibiting osteoclastogenesis and proinflammatory cytokine release (61).

It is generally known that pure Mg has a low corrosion resistance. Corrosion resistance can be optimised by alloying and processing (1,47,48,53,66). Ca appears to be a favourable alloying element for Mg, as it improves corrosion resistance and exhibits good mechanical properties (52,54). However, a disadvantage of Ca is the observed loss of formability. In the preliminary material development study by S.S. Nene et.al, the formability was increased by adding a second alloying element, Li. Li promotes ductility and is the most active element of all three elements (Mg, Ca, Li) according to the galvanic series of metals (70).

In simulated body fluid, biocorrosion resistance was evaluated, which showed satisfactory results. This improved corrosion resistance (compared to binary Mg–Li alloy) was achieved by microstructural refinement using the presence of the harder Mg2Ca phase additional to Li and hot rolling. Generally, the microstructural refinement in Mg alloys reduces the likelihood of localised corrosion forming a protective layer of $Mg(OH)_2$ since more grain boundary area is then available (66,70,71). With an average grain structure of 5 μm metres, LX41 has a grain structure similar to ZX00 (2-3 μm) (72).

Comparing the degradation of LX41 to ZX00, LX41 shows a more homogeneous but faster degradation already from the beginning. ZX00 demonstrated an increase in volume at the first two time points (2 and 6 weeks) after implantation. The initial increase occurred due to formation of a corrosion layer that makes it difficult to distinguish between the implant and the bone in terms of evaluation. According to Witte et al. this newly formed corrosion layer consists mainly of Ca and phosphorus and is a product of the bone-implant interaction and Mg alloy degradation, respectively. Furthermore, they assume that this layer composed of Ca, phosphorus, $Mg(OH)_2$ and oxides plays an important role in slowing down alloy degradation (73). Even though no increase in implant volume was

observed for LX41, a homogeneous corrosion layer with degradation clods and reddish areas corresponding to a Ca and phosphate layer was identified by histology. In comparison with other Mg-based alloys such as ZX50 and WZ21, LX41 performed better in terms of degradation rate. Twelve weeks after implantation, ZX50 was completely dissolved. WZ21 also performed worse with a remaining initial pin volume of approx. 50% after 24 weeks. In contrast, 62.40% initial pin volume was measurable for LX41 after 24 weeks (74). However, the slowest degradation rate was still observable for ZX00 with an 85% remaining implant volume after 24 weeks (69).

In concern of LX41 and ZX00 surface development, we showed a significant increase in surface area 2 weeks after implantation. Based on previous studies, we suggest that the formation of a corrosion layer at the beginning of the implant degradation process actually correlates with the increase in surface area. However, distinction between the remaining implant material and degradation layer was not possible due to the low-resolution imaging method (73). Up to week 18, the surface area remained nearly constant for both materials. However, a constant increase in implant surface was observable from time point 12 to 24 for ZX00. In contrast, LX41 showed a significant drop in implant surface area from t18 to t24. If we add the relationship between surface area and volume to the extended analysis, we see an interesting switch for LX41. Both materials start with a comparable surface-to-volume ratio of 2.9mm^{-1} for ZX00 and 3.02mm^{-1} for LX41. Furthermore, ZX00 showed a moderate increase of this ratio is evident, i.e. 3.73mm^{-1} at t18 and 4.16mm^{-1} at t24. Regarding LX41, a different pattern was observed. A significant increase in surface-to-volume ratio of 5.0mm^{-1} at time t18 was calculated. This can be explained due to the existing stable surface area and the ongoing volume degradation. At time point 24, this ratio actually dropped to only 4.55mm^{-1} and thereby became very similar to the ratio of ZX00 (69). The drastic decrease in surface area after 24 weeks and the significantly slower rate of degradation (average volume: t18-9.77mm^2 and t24 -9.49mm^2) led to the stabilisation of the degradation process. After initially faster degradation with multiple lacunar degradation, these results indicate a more homogeneous degeneration for LX41 occurs starting from 18 weeks on.

Another important parameter for comparison is gas evolution. Whenever Mg decomposes under physiological conditions, H_2 and $Mg(OH)_2$ are produced. Mg hydroxide surrounds the implant as a protective layer ($Mg+H_20=>Mg(OH)_2+H^2$) (57). H^2, on the other hand, is

released and is visible as gas bubbles next to the implant in µCT images or histology. Back in history, a strong gas formation was already macroscopically observable in the soft tissue, however, this is no longer the case nowadays (1). Grün et al. showed moderate gas development for ZX00 in the diaphysis of the femur, which peaked after 12 and 18 weeks. Gas development, which is mainly caused by stress corrosion, was particularly evident in the surrounding tissue (54). We showed a high gas evolution 2 weeks after implantation with 15.72mm^3 ± 9.87 SD, which, however, significantly decreased already 12 weeks post-surgery and showed comparable values to ZX00 after 18 and 24 weeks. Similarly to ZX00, we generally observed a preferential gas development in the trabecular bone and less in the cortical area (54). Despite the high gas development values at t2, no disturbances in bone formation were observed over the entire study period.

In our study, we calculated a degradation rate of 0.26mm/year. This degradation value is within the slower degradation range for Mg-based implants (range 0.08-1.56mm/year). AZ31, for example, decays at 1.17mm/year, WE43 at 1.56mm/year and LAE442 at 0.39mm/year (48). Currently, the lowest degradation rate was achieved with ZX00, which degraded at 0.08mm/year after implantation into the diaphysis of rat femur (54). It is important to consider the site of implantation when comparing degradation rates, as the degradation rate appears to be higher in the epiphysis than in the metaphysis and even slower in the diaphyseal area (74).

The histological evaluation of rat tibiae with LX41 implants and ZX00 were histologically comparable to the results obtained by Grün et al. There were no sclerotic areas or multinucleated giant cells, thereby negating a foreign body reaction occurring in the bone tissue surrounding the implant (54). In literature, these reactions have been described mainly in cases of too rapid degradation (75,76). Furthermore, new bone formation around the implant could be detected. Despite the more prominent gas development of LX41, the bone marrow cavity appeared to be intact in all areas like in ZX00. Due to the degradation of LX41, a corrosion layer with degradation clods were preferentially visible at the pin ends, but also along the pin. The prominent degradation clods of LX41 were more pronounced compared to the histological images of ZX00, which is probably due to the higher degradation rate (54). A uniform corrosion mechanism found *in vitro* was also shown histologically in our *in vivo* experimental setup. However, in addition to the uniform degradation, our *in vivo* model also showed several lacunar degradations per pin.

Despite the good combination of high specific force (142kN m/kg) and *in vitro* corrosion resistance, a faster degradation rate was calculated compared to ZX00 (70). One of the pins showed a very rapid degradation from time 18 onwards, whereupon this pin could no longer be evaluated for the last time point. The pin was still present to a certain extent, but a meaningful evaluation was not possible.

In literature, another application method for Li can be found. Li is not added to the stabilisation material, instead it is administered orally to strengthen the osteoporotic bone. Vachhani K. et. al orally treated rats post-fracture surgery with low-dose Li, evaluating the healing of osteoporotic fractures. The Li group received 20mg/kg/day for 14 days starting at day 7 or 10 post surgery. The control group was just treated with saline orally. Stereology and torsional mechanical testings were executed after 4 weeks for the day 7 onset regime and after 6 weeks for the day 10 onset treatment, in comparison to the placebo group. After 6 weeks, the maximum yield torque in the day 10 onset group was 50% higher than in the placebo group (309N-mm vs. 206N-mm). Starting with Li on day 7 led to a modest improvement in maximum yield torque, which might be owed to the earlier measurement in week 4. Furthermore, better periosteal and mineralized callus bridging was detected in the Li-treated femurs in general (65).

In summary, the degradation rate of LX41 revealed to be more rapid than in ZX00, even though adequate gas formation and osseointegration within a study duration of six months was observed in most pins.

6 Conclusion

Here we demonstrated an initially increased implant degradation and volume decrease of the LX41 implants in healthy growing rats. The gas formation and quantity was also primarily higher than that of the comparative material ZX00. However, there were no negative effects on bone healing and new bone formation. Considering the entire duration of the study, LX41 achieved very similar values to ZX00 from week 18 until the end of the study in terms of volume loss and the amount of gas produced. This decreasing degradation rate towards the end of the study, together with the good osseous integration and new bone formation, suggests that LX41 does have potential for the fixation of orthopaedic fractures. Furthermore, it is still uncertain whether osteoporotic bones benefit from LX41 degradation due to the released Mg, Ca and Li. Therefore, long-term studies are necessary to investigate the degradation behaviour of LX41 and due to the beneficial effect of Li on the elderly population, further studies in osteoporotic conditions are warranted.

7 References

1. Witte F. Reprint of: The history of biodegradable magnesium implants: A review. Acta Biomater. September 2015;23 Suppl:S28-40.
2. SEELIG MG. A STUDY OF MAGNESIUM WIRE AS AN ABSORBABLE SUTURE AND LIGATURE MATERIAL. Arch Surg. 1. März 1924;8(2):669–80.
3. Kamrani S, Fleck C. Biodegradable magnesium alloys as temporary orthopaedic implants: a review. Biometals Int J Role Met Ions Biol Biochem Med. April 2019;32(2):185–93.
4. Okuma T. Magnesium and bone strength. Nutr Burbank Los Angel Cty Calif. 2001;17(7–8):679–80.
5. Rahim MI, Eifler R, Rais B, Mueller PP. Alkalization is responsible for antibacterial effects of corroding magnesium. J Biomed Mater Res A. November 2015;103(11):3526–32.
6. Amerstorfer F, Fischerauer SF, Fischer L, Eichler J, Draxler J, Zitek A, et. al. Long-term in vivo degradation behavior and near-implant distribution of resorbed elements for magnesium alloys WZ21 and ZX50. Acta Biomater. 15. September 2016;42:440–50.
7. Galli S, Stocchero M, Andersson M, Karlsson J, He W, Lilin T, u. a. The effect of magnesium on early osseointegration in osteoporotic bone: a histological and gene expression investigation. Osteoporos Int J Establ Result Coop Eur Found Osteoporos Natl Osteoporos Found USA. Juli 2017;28(7):2195–205.
8. Lu C, Miclau T, Hu D, Hansen E, Tsui K, Puttlitz C, u. a. Cellular basis for age-related changes in fracture repair. J Orthop Res. 2005;23(6):1300–7.
9. Yang Y, He C, Dianyu E, Yang W, Qi F, Xie D, u. a. Mg bone implant: Features, developments and perspectives. Mater Des. 2020;185:108259.
10. Kim Y-K, Lee K-B, Kim S-Y, Bode K, Jang Y-S, Kwon T-Y, u. a. Gas formation and biological effects of biodegradable magnesium in a preclinical and clinical observation. Sci Technol Adv Mater. 9. April 2018;19(1):324–35.
11. Cohen MM. The new bone biology: pathologic, molecular, and clinical correlates. Am J Med Genet A. 1. Dezember 2006;140(23):2646–706.
12. Boyle WJ, Simonet WS, Lacey DL. Osteoclast differentiation and activation. Nature. 15. Mai 2003;423(6937):337–42.
13. Ross FP, Teitelbaum SL. alphavbeta3 and macrophage colony-stimulating factor: partners in osteoclast biology. Immunol Rev. Dezember 2005;208:88–105.
14. Lüllmann-Rauch R, Paulsen F. Taschenlehrbuch Histologie. 2012. Thieme; 157–178 S.
15. Lewiecki EM. Role of sclerostin in bone and cartilage and its potential as a therapeutic target in bone diseases. Ther Adv Musculoskelet Dis. 2014;6(2):48–57.
16. Rausch V, Seybold D, Königshausen M, Köller M, Schildhauer TA, Geßmann J. Grundlagen der Knochenbruchheilung. Orthop. 2017;46(8):640–7.
17. Frost HM. Wolff's Law and bone's structural adaptations to mechanical usage: an overview for clinicians. Angle Orthod. 1994;64(3):175–88.
18. Ubara Y, Fushimi T, Tagami T, Sawa N, Hoshino J, Yokota M, u. a. Histomorphometric features of bone in patients with primary and secondary hypoparathyroidism. Kidney Int. 2003;63(5):1809–16.
19. Clarke B. Normal bone anatomy and physiology. Clin J Am Soc Nephrol. 2008;3(Supplement 3):S131–9.
20. Reddy SV. Regulatory mechanisms operative in osteoclasts. Crit Rev Eukaryot Gene Expr. 2004;14(4).

21. Delaissé J-M, Andersen TL, Engsig MT, Henriksen K, Troen T, Blavier L. Matrix metalloproteinases (MMP) and cathepsin K contribute differently to osteoclastic activities. Microsc Res Tech. 2003;61(6):504–13.
22. Locklin RM, Oreffo RO, Triffitt JT. Effects of TGFβ and bFGF on the differentiation of human bone marrow stromal fibroblasts. Cell Biol Int. 1999;23(3):185–94.
23. Anderson HC. Matrix vesicles and calcification. Curr Rheumatol Rep. 2003;5(3):222–6.
24. Shaker JL, Deftos L. Calcium and Phosphate Homeostasis. In: Feingold KR, Anawalt B, Boyce A, Chrousos G, de Herder WW, Dhatariya K, u. a., Herausgeber. Endotext [Internet]. South Dartmouth (MA): MDText.com, Inc.; 2000 [zitiert 26. Oktober 2021]. Verfügbar unter: http://www.ncbi.nlm.nih.gov/books/NBK279023/
25. Kurtz A, Pape HC, Silbernagl S. Physiologie. 8. Georg Thieme Verlag, Stuttgart; 2018. 464–469 S.
26. Castiglioni S, Cazzaniga A, Albisetti W, Maier JAM. Magnesium and Osteoporosis: Current State of Knowledge and Future Research Directions. Nutrients. 31. Juli 2013;5(8):3022–33.
27. Miazgowski T, Kleerekoper M, Felsenberg D, Štěpán JJ, Szulc P. Secondary Osteoporosis: Endocrine and Metabolic Causes of Bone Mass Deterioration. J Osteoporos. 2012;2012:907214.
28. Sommer NG, Weinberg A-M. Die Rolle von Magnesium bei Knochenbrüchen in übergewichtigen Kindern und Jugendlichen. J Für Miner Muskuloskelettale Erkrank. 2021;1–7.
29. Health NI of. NIH consensus development panel on osteoporosis prevention, diagnosis, and therapy, March 7-29, 2000: highlights of the conference. South Med J. 2001;94(6):569–73.
30. Osteoporose | ÖGKM – Österreichische Gesellschaft für Knochen- und Mineralstoffwechsel [Internet]. [zitiert 26. Oktober 2021]. Verfügbar unter: https://www.oegkm.at/knochen/osteoporose/
31. Osteoporose [Internet]. [zitiert 26. Oktober 2021]. Verfügbar unter: http://www.osteoporose.co.at/begriffsdef.html
32. Zhang J, Cai L, Tang L, Zhang X, Yang L, Zheng K, u. a. Highly dispersed lithium doped mesoporous silica nanospheres regulating adhesion, proliferation, morphology, ALP activity and osteogenesis related gene expressions of BMSCs. Colloids Surf B Biointerfaces. 2018;170:563–71.
33. Böcker W, Denk H, Heitz PU, Moch H, Höfler G, Kreipe H. Lehrbuch Pathologie. Elsevier Health Sciences; 2019. 851–86 S.
34. Jahnen-Dechent W, Ketteler M. Magnesium basics. Clin Kidney J. 2012;5(Suppl_1):i3–14.
35. Saito N, Tabata N, Saito S, Andou Y, Onaga Y, Iwamitsu A, u. a. Bone mineral density, serum albumin and serum magnesium. J Am Coll Nutr. 2004;23(6):701S-703S.
36. Grifka J, Krämer J. Orthopädie Unfallchirurgie. Springer-Verlag; 2013. 74–76, 84–87 S.
37. Bastian O, Pillay J, Alblas J, Leenen L, Koenderman L, Blokhuis T. Systemic inflammation and fracture healing. J Leukoc Biol. 2011;89(5):669–73.
38. Kolar P, Gaber T, Perka C, Duda GN, Buttgereit F. Human early fracture hematoma is characterized by inflammation and hypoxia. Clin Orthop Relat Res. 2011;469(11):3118–26.
39. Neidlinger-Wilke C, Stalla I, Claes L, Brand R, Hoellen I, Rübenacker S, u. a. Human osteoblasts from younger normal and osteoporotic donors show differences in

proliferation and TGFβ-release in response to cyclic strain. J Biomech. 1995;28(12):1411–8.
40. Rivard A, Fabre J-E, Silver M, Chen D, Murohara T, Kearney M, u. a. Age-dependent impairment of angiogenesis. Circulation. 1999;99(1):111–20.
41. Stenderup K, Justesen J, Clausen C, Kassem M. Aging is associated with decreased maximal life span and accelerated senescence of bone marrow stromal cells. Bone. 2003;33(6):919–26.
42. Xing Z, Lu C, Hu D, Miclau III T, Marcucio RS. Rejuvenation of the inflammatory system stimulates fracture repair in aged mice. J Orthop Res. 2010;28(8):1000–6.
43. Lu C, Hansen E, Sapozhnikova A, Hu D, Miclau T, Marcucio RS. Effect of age on vascularization during fracture repair. J Orthop Res. 2008;26(10):1384–9.
44. Lu C, Saless N, Wang X, Sinha A, Decker S, Kazakia G, u. a. The role of oxygen during fracture healing. Bone. 2013;52(1):220–9.
45. Hirner A, Weise K. Chirurgie: Schnitt für Schnitt. Georg Thieme Verlag; 2004. 232–235 S.
46. Thomsen M, Thomas P. Verträglichkeit und Allergie von Osteosynthesematerialien. Unfallchirurg. 2017;120(2):116–21.
47. Myrissa A, Agha NA, Lu Y, Martinelli E, Eichler J, Szakacs G, u. a. In vitro and in vivo comparison of binary Mg alloys and pure Mg. Mater Sci Eng C. 2016;61:865–74.
48. Zhao D, Witte F, Lu F, Wang J, Li J, Qin L. Current status on clinical applications of magnesium-based orthopaedic implants: A review from clinical translational perspective. Biomaterials. 2017;112:287–302.
49. Luo Y, Zhang C, Wang J, Liu F, Chau KW, Qin L, u. a. Clinical translation and challenges of biodegradable magnesium-based interference screws in ACL reconstruction. Bioact Mater. 2021;6(10):3231–43.
50. Jingyuan Y, Jianzhong W, Qiang L, Jian S, Jianming C, Xudong S. Effect of Zn on microstructures and properties of Mg-Zn alloys prepared by powder metallurgy method. Rare Met Mater Eng. 2016;45(11):2757–62.
51. Tie D, Feyerabend F, Hort N, Hoeche D, Kainer KU, Willumeit R, u. a. In vitro mechanical and corrosion properties of biodegradable Mg–Ag alloys. Mater Corros. 2014;65(6):569–76.
52. Li Z, Gu X, Lou S, Zheng Y. The development of binary Mg–Ca alloys for use as biodegradable materials within bone. Biomaterials. 2008;29(10):1329–44.
53. Ben-Hamu G, Eliezer D, Kaya A, Na YG, Shin KS. Microstructure and corrosion behavior of Mg–Zn–Ag alloys. Mater Sci Eng A. 2006;435:579–87.
54. Grün NG, Holweg P, Tangl S, Eichler J, Berger L, van den Beucken JJJP, u. a. Comparison of a resorbable magnesium implant in small and large growing-animal models. Acta Biomater. 15. September 2018;78:378–86.
55. Holweg P, Berger L, Cihova M, Donohue N, Clement B, Schwarze U, u. a. A lean magnesium–zinc–calcium alloy ZX00 used for bone fracture stabilization in a large growing-animal model. Acta Biomater. 2020;113:646–59.
56. Herber V, Labmayr V, Sommer NG, Marek R, Wittig U, Leithner A, u. a. Can Hardware Removal be Avoided Using Bioresorbable Mg-Zn-Ca Screws After Medial Malleolar Fracture Fixation? Mid-Term Results of a First-In-Human Study. Injury. 2021;
57. Gonzalez J, Hou RQ, Nidadavolu EP, Willumeit-Römer R, Feyerabend F. Magnesium degradation under physiological conditions–Best practice. Bioact Mater. 2018;3(2):174–85.
58. Sanchez AHM, Luthringer BJ, Feyerabend F, Willumeit R. Mg and Mg alloys: how comparable are in vitro and in vivo corrosion rates? A review. Acta Biomater. 2015;13:16–31.

59. McIntyre RS, Berk M, Brietzke E, Goldstein BI, López-Jaramillo C, Kessing LV, u. a. Bipolar disorders. The Lancet. 2020;396(10265):1841–56.
60. Nam D, Balasuberamaniam P, Milner K, Kunz M, Vachhani K, Kiss A, u. a. Lithium for Fracture Treatment (LiFT): a double-blind randomised control trial protocol. BMJ Open. 2020;10(1):e031545.
61. Pan C, Chen L, Wu R, Shan H, Zhou Z, Lin Y, u. a. Correction: Lithium-containing biomaterials inhibit osteoclastogenesis of macrophages in vitro and osteolysis in vivo. J Mater Chem B. 2019;7(15):2566–2566.
62. Ma Y, Li Y, Hao J, Ma B, Di T, Dong H. Evaluation of the degradation, biocompatibility and osteogenesis behavior of lithium-doped calcium polyphosphate for bone tissue engineering. Biomed Mater Eng. 2019;30(1):23–36.
63. Luo Y, Li D, Zhao J, Yang Z, Kang P. In vivo evaluation of porous lithium-doped hydroxyapatite scaffolds for the treatment of bone defect. Biomed Mater Eng. 2018;29(6):699–721.
64. Hu X, Wang Z, Shi J, Guo X, Wang L, Ping Z, u. a. Lithium chloride inhibits titanium particle-induced osteoclastogenesis by inhibiting the NF-κB pathway. Oncotarget. 2017;8(48):83949.
65. Vachhani K, Whyne C, Wang Y, Burns DM, Nam D. Low-dose lithium regimen enhances endochondral fracture healing in osteoporotic rodent bone. J Orthop Res. 2018;36(6):1783–9.
66. Jin Y, Blawert C, Yang H, Wiese B, Feyerabend F, Bohlen J, u. a. Microstructure-corrosion behaviour relationship of micro-alloyed Mg-0.5 Zn alloy with the addition of Ca, Sr, Ag, In and Cu. Mater Des. 2020;195:108980.
67. Donath K. Die Trenn-Dünnschliff-Technik zur Herstellung histologischer Präparate von nicht schneidbaren Geweben und Materialien: Apparate-und Methodenbeschreibung. EXAKT-Kulzer-Druckschr.; 1988.
68. Lackó J, Géza L. A simple differential staining method for semi-thin sections of ossifying cartilage and bone tissues embedded in epoxy resin. Mikroskopie. 1975;31:1–4.
69. Paar L. Evaluation of a magnesium-based implant in the growing rat model. [Graz]: Medizinischen Universität Graz; 2022.
70. Nene SS, Kashyap BP, Prabhu N, Estrin Y, Al-Samman T. Microstructure refinement and its effect on specific strength and bio-corrosion resistance in ultralight Mg–4Li–1Ca (LC41) alloy by hot rolling. J Alloys Compd. 2014;615:501–6.
71. Zeng R-C, Sun L, Zheng Y-F, Cui H-Z, Han E-H. Corrosion and characterisation of dual phase Mg–Li–Ca alloy in Hank's solution: The influence of microstructural features. Corros Sci. 2014;79:69–82.
72. Brunner P, Brumbauer F, Steyskal E-M, Renk O, Weinberg A-M, Schroettner H, u. a. Influence of high-pressure torsion deformation on the corrosion behaviour of a bioresorbable Mg-based alloy studied by positron annihilation. Biomater Sci. 2021;
73. Witte F, Kaese V, Haferkamp H, Switzer E, Meyer-Lindenberg A, Wirth CJ, u. a. In vivo corrosion of four magnesium alloys and the associated bone response. Biomaterials. 2005;26(17):3557–63.
74. Kraus T, Fischerauer S, Treichler S, Martinelli E, Eichler J, Myrissa A, u. a. The influence of biodegradable magnesium implants on the growth plate. Acta Biomater. 2018;66:109–17.
75. Makkar P, Sarkar SK, Padalhin AR, Moon B-G, Lee YS, Lee BT. In vitro and in vivo assessment of biomedical Mg–Ca alloys for bone implant applications. J Appl Biomater Funct Mater. 2018;16(3):126–36.
76. Cheng M, Wahafu T, Jiang G, Liu W, Qiao Y, Peng X, u. a. A novel open-porous magnesium scaffold with controllable microstructures and properties for bone regeneration. Sci Rep. 2016;6(1):1–14.